

## APPLIED PHYSICS REVIEWS—FOCUSED REVIEW

**Schottky barriers in carbon nanotube-metal contacts**Johannes Svensson<sup>1</sup> and Eleanor E. B. Campbell<sup>2,a)</sup><sup>1</sup>*Electrical and Information Technology, Lund University, Box 118, SE-22100, Sweden*<sup>2</sup>*EaStCHEM, School of Chemistry, Edinburgh University, Edinburgh EH9 3JJ, Scotland**and Division of Quantum Phases and Devices, School of Physics, Konkuk University, Seoul 143-701, South Korea*

(Received 1 July 2011; accepted 1 November 2011; published online 8 December 2011)

Semiconducting carbon nanotubes (CNTs) have several properties that are advantageous for field effect transistors such as high mobility, good electrostatics due to their small diameter allowing for aggressive gate length scaling and capability to withstand high current densities. However, in spite of the exceptional performance of single transistors only a few simple circuits and logic gates using CNTs have been demonstrated so far. One of the major obstacles for large scale integration of CNTs is to reliably fabricate p-type and n-type ohmic contacts. To achieve this, the nature of Schottky barriers that often form between metals and small diameter CNTs has to be fully understood. However, since experimental techniques commonly used to study contacts to bulk materials cannot be exploited and studies often have been performed on only single or a few devices there is a large discrepancy in the Schottky barrier heights reported and also several contradicting conclusions. This paper presents a comprehensive review of both theoretical and experimental results on CNT-metal contacts. The main focus is on comparisons between theoretical predictions and experimental results and identifying what needs to be done to gain further understanding of Schottky barriers in CNT-metal contacts. © 2011 American Institute of Physics. [doi:[10.1063/1.3664139](https://doi.org/10.1063/1.3664139)]

**TABLE OF CONTENTS**

I. INTRODUCTION .....	1
II. ELECTRONIC PROPERTIES OF CARBON NANOTUBES .....	2
III. SCHOTTKY BARRIER FUNDAMENTALS ..	3
IV. THEORETICAL MODELING OF CNT-METAL CONTACTS.....	4
A. Electrostatic modeling .....	5
B. Density functional theory modeling.....	6
V. SCHOTTKY BARRIER HEIGHT MEASUREMENT TECHNIQUES .....	8
VI. EXPERIMENTAL STUDIES OF CNT-METAL CONTACTS .....	9
A. Measurements of Schottky barrier heights ..	9
B. Imaging of depletion region .....	13
VII. CONCLUSIONS .....	14

**I. INTRODUCTION**

The rapid development of integrated circuits for logic computation, with a doubling of the number of transistors on a processor chip every two years, a trend known as Moore's law,<sup>1,2</sup> has to a large extent been enabled due to the improvement of Si transistors. By scaling down dimensions, increasing

charge mobility by introducing strain in the material, using gate dielectrics with high dielectric constants, and designing new gating geometries, the performance of Si transistors has been pushed close to its physical limits. An indefinite continuation of the improvement is impossible since leakage currents increase power consumption and the electrostatics of small devices that lead to short channel effects, degrade the performance as transistor dimensions are further reduced. Due to the large economic incentive in the performance improvement of computers, both industry and academia are putting a lot of effort into the research of new materials suitable to replace Si by offering superior current transport properties and improved electrostatics.

One of the most promising materials to replace Si in high speed transistors is carbon in the form of one dimensional carbon nanotubes<sup>3</sup> (CNTs) and two dimensional graphene.<sup>4</sup> Of these two, CNTs are the more suitable choice for transistors for logic computation which requires a large difference in current between the on and the off-states since two thirds of all CNTs have a sufficiently large intrinsic band gap. In contrast, graphene which is a semimetal has to be geometrically<sup>5–7</sup> or chemically<sup>8,9</sup> modified to induce a band gap and is therefore more suited for radio frequency (RF) applications.<sup>10</sup>

In spite of the impressive intrinsic electronic properties<sup>11</sup> and promising performance of single CNT transistors there are still many issues that have to be solved before CNT field effect transistors (CNTFETs) can make the transition

<sup>a)</sup>Electronic mail: Eleanor.Campbell@ed.ac.uk.

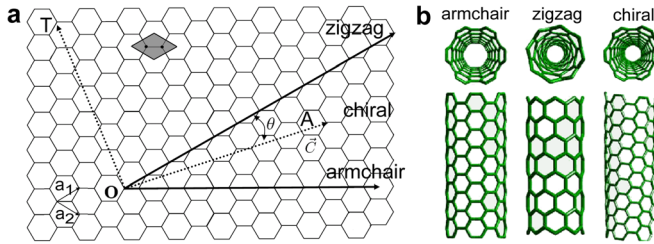


FIG. 1. (Color online) (a) Two dimensional hexagonal lattice with basis vectors indicated by  $\vec{a}_1$  and  $\vec{a}_2$ . A chiral CNT is conceptually formed by cutting the lattice along the vectors OT and OA and connecting points O and A by rolling it into a cylinder. The vector  $\vec{C} = n\vec{a}_1 + m\vec{a}_2$  defines the circumference of the CNT and  $\theta$  its chiral angle. The solid lines indicate the circumferences of a zigzag and an armchair CNT. The grey rhombus depicts a unit cell. (b) Examples of the three different types of CNTs. Adapted from X. Zhou, "Carbon nanotube transistors, sensors, and beyond," p 26, Ph.D. dissertation (Cornell University, 2008). Copyright © 2008, Cornell University Press.

from academic research to large scale industrial production. One of the obstacles for large scale integration is to achieve ohmic contacts between CNTs and metal electrodes to enable high on-state currents and improved switching of CNTFETs. Contacts with low Schottky barriers for both n (Ref. 12) and p-type (Ref. 13) CNTFETs have been realised for large diameter CNTs but a full understanding of what factors determine the Schottky barrier height is still lacking. In spite of a wealth of experimental and theoretical studies, there are still many contradictory results and predictions, mainly concerning the influence of interface states on the Schottky barrier height. Therefore, this focused review summarises both experimental and theoretical results on CNT-metal Schottky barriers and emphasizes and clarifies the various discrepancies that exist in the literature. Section II, which is a short introduction to the electronic properties of CNTs, is followed by an introduction to Schottky barriers in section three. The fourth section focuses on theoretical studies of CNT-metal Schottky barriers and the fifth section explains the different experimental techniques used to measure Schottky barrier heights and presents the available experimental results obtained in the literature. Finally, in chapter six, a discussion on what experimental studies are need to gain a deeper understanding of Schottky barriers in metal-CNTs contacts is presented.

## II. ELECTRONIC PROPERTIES OF CARBON NANOTUBES

Single walled carbon nanotubes (SWCNTs), discovered in 1993,<sup>14</sup> are hollow cylinders of carbon with diameters in the range of a single to a few nanometers and with lengths up to 10 s of cm.<sup>15</sup> The structure of a CNT can be conceptually described by starting with a single sheet of graphite, known as graphene. Graphene consists of a hexagonal network of carbon atoms with three  $sp^2$  hybridised valence electrons that give rise to covalent in-plane  $\sigma$ -bonds while the remaining p-orbital gives rise to  $\pi$ -bonds. To form a CNT, a narrow strip is cut out from the graphene sheet in a specific direction and then rolled into a seamless cylinder (Figure 1). Depending on the direction the sheet is cut, the CNT will

have a different chirality affecting mainly its electronic properties. By taking the unit vectors of the hexagonal planar lattice and multiplying by the integers  $m$  and  $n$  a resulting vector  $\vec{C} = n\vec{a}_1 + m\vec{a}_2$  is obtained which defines the circumference of the CNT.  $m$  and  $n$  are called the chirality indices and uniquely determine the structure of the CNT. CNTs with indices  $n=m$  are called armchair, those with  $n=0$  zigzag and the rest are referred to as chiral tubes.

The electronic properties of CNTs can be derived from those of graphene which has a conical dispersion around the Fermi level and is a semi-metal, i.e., it has no band gap but its density of states (DOS) goes to zero at the Fermi level. As the graphene sheet is rolled up into a CNT, the wavefunctions of the electrons are confined around its circumference. Since a periodic boundary condition is now imposed on the electron wave functions only discrete wave vectors that fulfill  $\vec{k}_\perp \cdot \vec{C} = \pi dk_\perp = 2\pi i$ , where  $d$  is the CNT diameter and  $i$  is an integer, are allowed along the circumference of the CNT. This boundary condition on the wavefunctions in a CNT gives slices of allowed k-values in the conical band structure of graphene (Figure 2(a)). The position of the slices is determined by the chirality of the CNT. If a slice crosses the K and K' points where the valence and conduction bands meet at the Fermi energy, the CNT has bands with a linear dispersion relation and is metallic (Figure 2(b)). In contrast, if no slice crosses the K and K' points, the CNT has bands that are parabolic close to the Fermi level and has an energy band gap in between them, i.e., it is semiconducting (Figure 2(c)). The energy dispersion of the bands close to the Fermi level is given by

$$E(k) = \pm \left( (\hbar v_F k)^2 + (E_g/2)^2 \right)^{1/2}, \quad (1)$$

where  $v_F = 8 \cdot 10^5$  m/s is the Fermi velocity and  $E_g = 2a_{C-C}\gamma_0/d$  is the band gap where  $a_{C-C} = 1.42$  Å is the nearest neighbour distance in the hexagonal lattice,  $\gamma_0 = 2.9$  eV the tight-binding overlap integral and  $d$  the diameter.<sup>17</sup> It should, however, be noted that there is a large discrepancy in calculated and measured proportionality constants  $2a_{C-C} \cdot \gamma_0$  between the band gap and inverse diameter with values between 0.71 and 1.1 reported.<sup>18,19</sup>

If only the circumferential confinement of the wave functions is considered, CNTs with chirality indices that fulfill the requirement  $n - m = 3p$  where  $p$  is an integer are metallic and those that fulfill  $n - m \neq 3p$  are semiconducting. However, the curvature of the CNT wall<sup>22</sup> or mechanical deformations<sup>23,24</sup> of the CNT may induce band gaps of a few 10 s of mV also in otherwise metallic CNTs.

Since electrons can only scatter either backward or forward in the quasi one dimensional CNTs, the mean free path between two scattering events is considerably longer than in higher dimensions where scattering in all directions is possible. This low scattering probability leads to mean free paths of up to a  $\mu$ m in semiconducting CNTs for low electric fields resulting in field effect mobilities larger than  $100\,000$  cm $^2$ /Vs at 50 K.<sup>11</sup> For low longitudinal electric fields, the dominating scattering mechanism is emission of acoustic phonons with a mean free path of  $l_{mfp} = 300$  nm–1.5  $\mu$ m.<sup>25,26</sup> At high electric fields, the electrons gain enough energy to emit optical

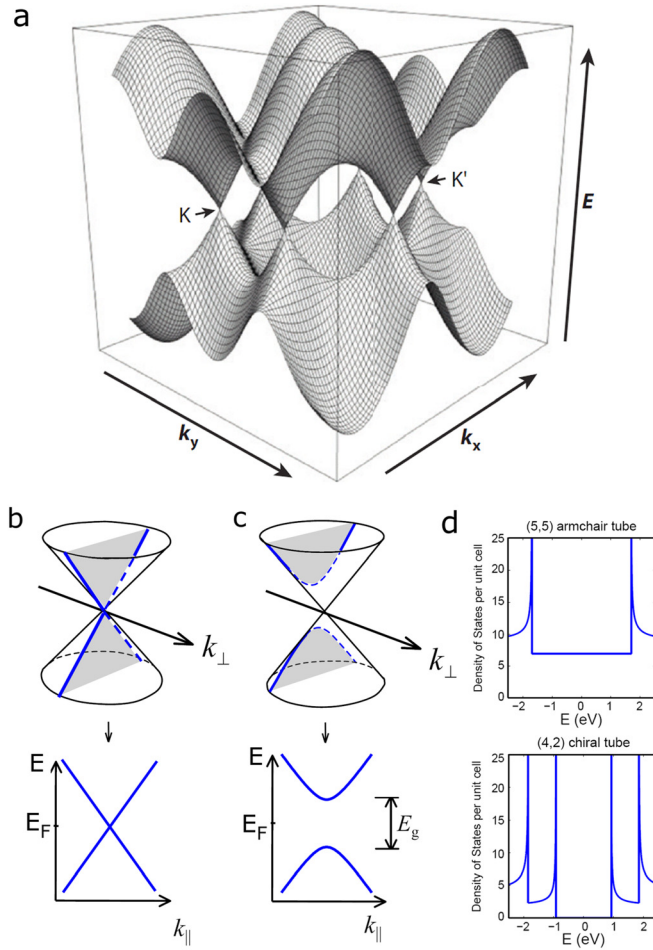


FIG. 2. (Color online) (a) The band dispersion of graphene.  $k_x$  and  $k_y$  are the wave vectors in the plane and  $E$  is the energy. The bands meet at the  $K$  points around which the dispersion is conical.<sup>20</sup> (b) The conical band structure of graphene with a slice of allowed wave vectors  $k_{\perp}$  that pass through the point where the two bands meet at the Fermi level. This gives the 1D band structure of a metallic CNT. (c) Slice of allowed  $k_{\perp}$  not passing through the point where the bands meet which gives the band structure of a semiconducting CNT. (d) DOS for a (5,5) metallic CNT with a finite DOS at the Fermi energy and a (4,2) semiconducting CNT with zero DOS around the Fermi energy. The peaks are van Hove singularities positioned at the edges of the subbands.<sup>21</sup> Image adapted from E. Minot, "Tuning the band structure of carbon nanotubes," Ph.D. dissertation (Cornell University, 2004). Copyright © 2004, Cornell University Press.

phonons which have stronger electron-phonon coupling and therefore the mean free path is reduced to 15 nm.<sup>26</sup>

The extraordinary high mobility in combination with their resilience to high current densities,<sup>27</sup> simple integration with various gate dielectrics<sup>28</sup> and good electrostatics due to their small diameter makes CNTs an attractive option for various electronic devices such as high speed transistors and Schottky diodes.

The first CNTFETs demonstrated in 1998 by Tans *et al.*<sup>29</sup> and Martel *et al.*<sup>30</sup> were initially believed to operate in a similar way as conventional MOSFETs where the potential in the bulk of the channel is the most important factor that controls the current. However, it was soon discovered that Schottky barriers at the CNT-metal contacts were of great importance for the transport properties for many metal species.<sup>31</sup> In the following years, there were several studies, on the impact of the Schottky barriers on the transport properties of CNTFETs.<sup>32–35</sup>

Many CNTFETs exhibit a p-type behavior with dominant hole conduction in air but can be changed to n-type when put in vacuum. The mechanism behind this change is still not fully resolved. Derycke *et al.* deduced that the change of characteristics is mainly due to a change of the work function of the metal contact as oxygen is desorbed.<sup>33</sup> In contrast, Chen *et al.* concluded that the p-type behaviour observed in air is due to oxygen doping of the CNT and the work function of the metal is of less importance.<sup>34</sup> The importance of the substrate has also been highlighted by Aguirre *et al.* who used a hydrophobic polymer underneath the CNT to form ambipolar devices due to the lack of absorbed water.<sup>35</sup>

Since this review is focused on Schottky barriers in CNT-metal contacts, the reader further interested in the electronic properties of CNTs and CNTFETs is referred to some excellent reviews on the topic.<sup>20,38–42</sup>

### III. SCHOTTKY BARRIER FUNDAMENTALS

For transistor applications, a low Schottky barrier for either holes or electrons is preferable since that not only reduces the contact resistance but also results in a good on/off ratio and a small inverse subthreshold slope. In contrast, in Schottky diodes suitable for high frequency applications such as detectors, mixers, and frequency multipliers a sufficiently high Schottky barrier is required for good current rectification.<sup>43</sup> Therefore, to properly design CNT devices it is important to understand how Schottky barriers in CNT-metal contacts are formed and what factors influence their heights.

In this chapter, an introduction to the formation and transport physics of Schottky barriers is given with an emphasis on CNT-metal contacts. A more in-depth discussion of the physics of metal-semiconductor contacts can be found in Rhoderick<sup>44</sup> and in Monch.<sup>45</sup>

If a metal and a semiconductor are joined and the Fermi level in the semiconductor is higher in energy than that in the metal, electrons move from the semiconductor into the metal leaving a positive background of ionised atoms. Electrons continue to be transported across the interface until the Fermi levels of the two systems have equilibrated (Figure 3). A Schottky barrier for holes (electrons) arises due to the mismatch between the Fermi level of the metal and the valence (conduction) band of the semiconductor. According to the first theoretical descriptions of metal-semiconductor contacts by Schottky<sup>46</sup> and Mott,<sup>47</sup> the Schottky barrier height for electrons is given by

$$\Phi_{SBe} = \phi_m - \chi, \quad (2)$$

where  $\phi_m$  is the work function of the metal which is the energy needed to remove an electron from the Fermi level into vacuum and  $\chi$  is the electron affinity of the semiconductor which is the energy needed to remove an electron from the bottom of the conduction band. Consequently, the barrier height for holes is given by

$$\Phi_{SBh} = \chi + E_g - \phi_m = I_s - \Phi_m, \quad (3)$$

where  $E_g$  is the band gap and  $I_s$  the ionisation potential of the semiconductor which corresponds to the energy difference between the top of the valence band and vacuum.

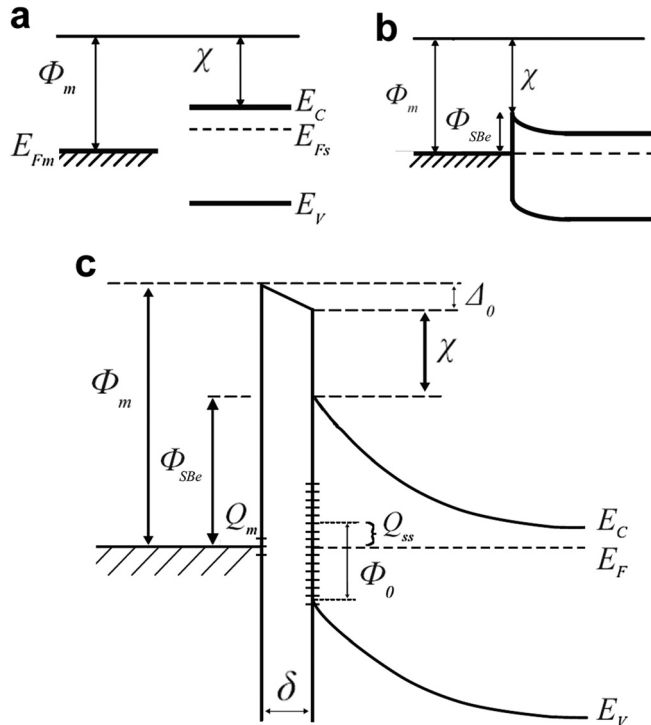


FIG. 3. (a) Energy band diagram before contact is made between a metal and a n-type semiconductor. (b) When contact is made, the Fermi levels equilibrate and a Schottky barrier arise. The image depicts a case without interface states. (c) Energy band diagram of a contact between a metal and a n-type semiconductor with interface states in the band gap at the semiconductor surface. The charge  $Q_{ss}$  in the interface states creates a dipole over a distance  $\delta$  that lowers the barrier height by  $\Delta_0$ . The notations used are defined in the main text.<sup>54</sup> Adapted from J. Piscator, "Influence of electron charge states in nanoelectronic building blocks," Ph.D. dissertation, (Chalmers University of Technology, 2009). Copyright © 2009, Johan Piscator.

However, it has been observed for many semiconductors that the Schottky barrier height has only a small dependence on the work function of the metal contact.<sup>48</sup> Thus, the Schottky barrier heights do not follow the simple relations in Eqs. (2) and (3) but instead have a much weaker dependence on the metal work function, a phenomenon known as Fermi-level pinning. This weak dependence has been attributed to interface states which have energies within the band gap of the semiconductor and are localized close to the contact (Figure 3(c)). These interface states arise because wavefunctions of the electrons in the metal are not abruptly terminated at the junction but extend a few Å into the surface of the semiconductor and are therefore referred to as metal-induced gap states (MIGS).<sup>49–51</sup>

It is possible to define a charge neutrality level  $\Phi_0$  for the interface states measured from the top of the valence band. States lower in energy than  $\Phi_0$  are of donor type and positively charged when empty and states higher in energy than  $\Phi_0$  are of acceptor type and negatively charged when full. This means that if the Fermi level of the semiconductor coincides with  $\Phi_0$ , there is no charge trapped in the interface states but if it is above or below  $\Phi_0$  the surface has a negative or positive charge  $Q_{ss}$ , respectively. In order to preserve charge neutrality,  $Q_{ss}$  together with any space charge in the depletion layer ( $Q_{sc}$ ), has to be balanced by an equal amount of charge of opposite sign on the metal surface ( $Q_m$ ), i.e.,

$Q_m + Q_{ss} + Q_{sc} = 0$ . This charge transfer results in a dipole over a distance  $\delta$  of atomic dimensions. The potential drop over this dipole modifies the Schottky barrier height from the Schottky-Mott relation in Eq. (2). Therefore, in the presence of interface states, the Schottky barrier height for electrons can instead be described by

$$\Phi_{SBe} = \gamma(\Phi_m - \chi) + (1 - \gamma)(E_g - \Phi_0), \quad (4)$$

where

$$\gamma = \frac{1}{1 + \frac{qD_{it}\delta}{\epsilon_i}}, \quad (5)$$

$\epsilon_i$  is the permittivity of the interface and  $D_{it}$  the density of interface states.<sup>48</sup> If  $D_{it}$  is large,  $\gamma \rightarrow 0$  and the Schottky barrier height approaches  $\Phi_{SBe} = E_g - \Phi_0$  and is thus determined entirely by the interface states and is completely independent of metal work function while in the absence of interface states,  $\gamma \rightarrow 1$  and the Schottky-Mott limit described by Eq. (2) is obtained. The variation of the Schottky barrier height as a function of the metal work function ( $\partial\Phi_{SBe}/\partial\Phi_m$ ) for different metal contacts on a given semiconductor gives a measure of the strength of the Fermi level pinning and can in principle be used to estimate  $D_{it}$ .

However, that MIGS is the main reason for the formation of the interface dipole has been disputed by, e.g., the proponents of chemical bond polarisation theory.<sup>52,53</sup> According to this theory, the most significant effect that gives rise to the dipole that alters the Schottky barrier height from the Schottky-Mott limit is the charge rearrangement that occurs when bonds are formed and not interface states. The chemical bond polarisation theory gives a similar description of the Schottky barrier height as Eq. (4) but where  $\gamma$  depends on the density of bonds instead of the density of interface states.

Due to Fermi level pinning, it is difficult to predict the Schottky barrier height of a certain metal-semiconductor combination from the properties of the separate materials, something which is desirable for many applications. However, it is possible to control the Schottky barrier height through passivation of the semiconductor surface to remove dangling bonds prior to metal deposition<sup>55</sup> or by introducing polar molecules at the interface.<sup>56</sup>

#### IV. THEORETICAL MODELING OF CNT-METAL CONTACTS

The Schottky barriers between CNTs and different metals have been studied theoretically by electrostatic modeling where the potential distribution is calculated for bulk objects with a defined charge distribution which gives the energy of the bands and the Schottky barrier heights.<sup>57–60</sup> In these calculations, the CNT is considered to be an ideal cylinder and the exact atomic configuration is disregarded.

The main benefit of this method is that device dimensions resembling those of experimental devices can easily be modeled. It is also relatively straightforward to include dielectrics and gates and calculate current-voltage characteristics.<sup>61</sup>

Another popular approach is to use density functional theory (DFT) modeling that calculates the charge density distribution on a microscopic scale. Even though DFT takes the exact atomic arrangement at the contact into account, and therefore allows the use of different CNT chiralities and crystal orientations of the metal, it has the drawback that it is computationally intensive and therefore limited to only very small contacts and short CNTs.

A third method is to use tight binding calculations which are less accurate compared to DFT but have the benefit of allowing larger systems to be modeled and still take into account the atomic scale electronic structure.<sup>62</sup>

The theoretical studies often use an idealised contact geometry where a metal surface with a specific crystallographic orientation is either strongly covalently bonded to the dangling bonds at the ends of a CNT or has weak van der Waals bonds to the side of a CNT (Figure 4). However, DFT calculations by Maiti *et al.* suggest that for strong metal-CNT interactions the  $sp^2$  hybridised carbon orbitals may change to  $sp^3$  which allows for strong bonds with the metal, also in the side-bonded geometry.<sup>63</sup> Even though there are some reports of end-bonded CNTs (Refs. 64 and 65), an overwhelming majority of the experimental studies have been performed on side bonded CNTs.

### A. Electrostatic modeling

One of the most influential theoretical studies on Schottky barriers in CNT-metal contacts has been performed by Léonard *et al.*<sup>57</sup> The authors consider an end-bonded configuration with a cylinder with a diameter of 1.4 nm which is terminated at a planar metal contact. The presence of dipoles

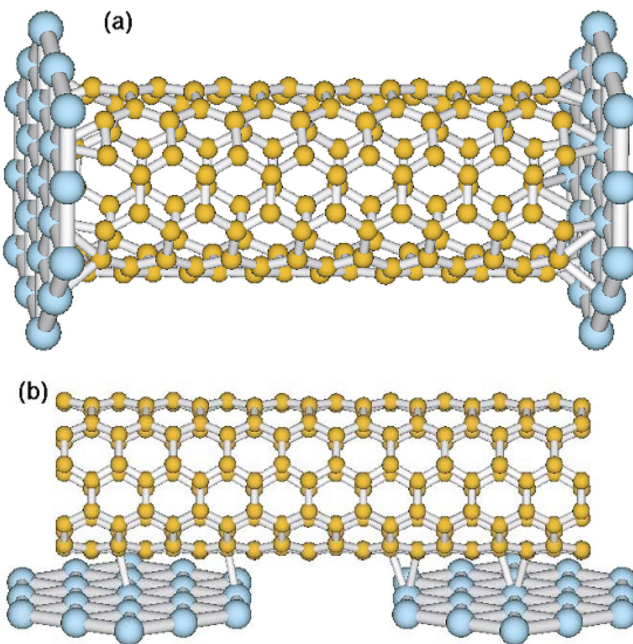


FIG. 4. (Color online) A (5,5) CNT contacted to a (111) metal surface with an end bonded (a) and a side bonded (b) configuration.<sup>66</sup> Reprinted with permission from J. J. Palacios, A. J. Pérez-Jiménez, E. Louis, E. SanFabián, and J. A. Vergés, Phys. Rev. Lett. **90**, 106801 (2003). Copyright © 2003, American Physical Society.

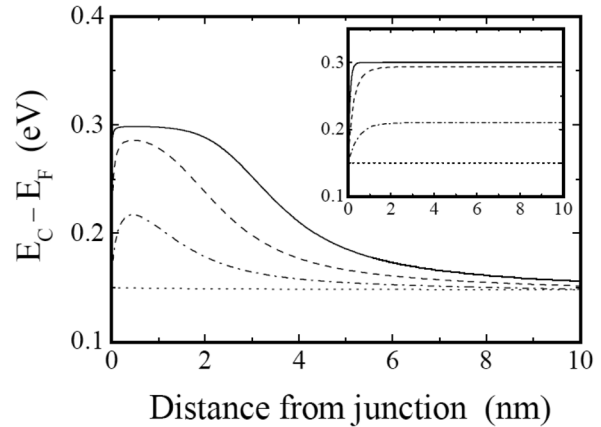


FIG. 5. Conduction band minimum as a function of distance from an end bonded CNT-metal junction for different densities of interface states. Dotted, dash-dotted, dashed, and solid lines are for 0, 0.01, 0.1, and 1 states/(atom-eV), respectively. The potential barrier induced by interface states decays within a few nm into the CNT. The inset shows the corresponding result for a planar junction where the interface states shift the bands far into the CNT. Reprinted with permission from F. Léonard and J. Tersoff, Phys. Rev. Lett. **84**, 4693 (2000). Copyright © 2000, American Physical Society.

due to interface states is taken into account by introducing charges that give rise to a potential that decays within a few nm. A high density of dipole charge corresponds to a large density of interface states ( $D_{it}$  in Eq. (5)) which is expected to pin the Fermi level. However, in contrast to a planar contact where the induced dipole sheet shifts the potential of the bands of the semiconductor also far away from the interface, the dipole in a metal-CNT contact is localised in all directions. Therefore, the interface states shift the bands within a depth of only a few nanometers from the junction creating a thin barrier while the energies of the bands deeper into the CNT are the same as for a contact without interface states (Figure 5). Since the potential barrier at the junction only extends a few nanometers into the CNT, electrons can easily tunnel through it so the interface states have little influence on the electrical behavior of the contact.

In addition to this study on end-bonded CNTs, Léonard *et al.*<sup>58</sup> have also considered a side contacted CNT modeled as a hollow cylinder embedded in a concentric metal shell. Since the depletion region for this geometry extends perpendicular to the main axis of the CNT there is only a short available distance on which the bands can realign to equilibrate the Fermi levels (Figure 3) and therefore only partial band realignment is possible. To study the effect of interface states on the Schottky barrier height, a sheet of pinning charge was also added at the surface of the CNT.

As the density of interface states increases, the increased pinning charge shifts the Schottky barrier height from its unperturbed initial value toward that of a fully pinned barrier (Figure 6). However, the added charge density has to be 100 times larger than in a 3-dimensional bulk contact to induce any pinning where a density of interface states of  $10^{-3}$  states/eV/atom is sufficient to significantly alter the Schottky barrier height. The reason for the weak pinning is that the pinning charge has to compete with the large charge density at the van Hove singularities in the DOS of the 1-dimensional CNT that are positioned at the band edges.

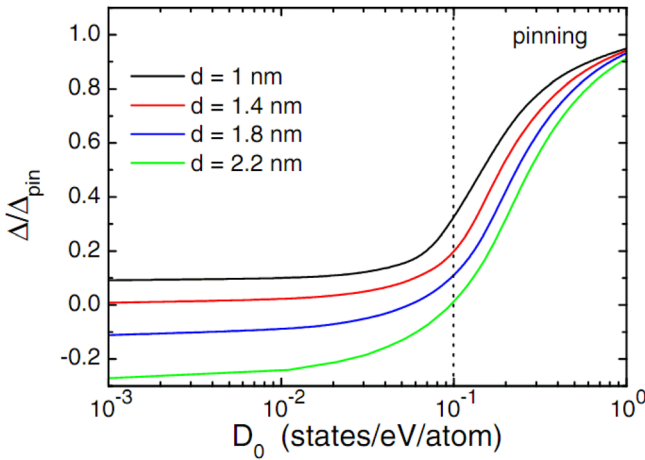


FIG. 6. (Color online) Ratio of the Schottky barrier height ( $\Delta$ ) and a Schottky barrier height when the Fermi level is pinned to the middle of the band gap ( $\Delta_{\text{pin}} = E_g/2$ ) as a function of the density of gap states for several CNTs of different diameter. Reprinted with permission from F. Léonard and A. A. Talin, Phys. Rev. Lett. **97**, 026804 (2006). Copyright © 2006, American Physical Society.

The two studies discussed above predict that the Schottky barrier height should be fully controlled by the metal work function in a CNT-metal contact in strong contrast to most bulk metal-semiconductor junctions where Fermi level pinning often dominates the Schottky barrier height. This is an attractive feature since it in principle allows CNT-metal junctions with a specific Schottky barrier height to be fabricated by selecting a suitable metal (Figure 7(b)). Since the band gap of a CNT  $E_g \propto 1/d$  the Schottky barrier heights for both holes and electrons are also expected to be inversely proportional to the diameter if the work function of CNTs is independent of their diameter (Figure 7(a)).

## B. Density functional theory modeling

In contrast to the electrostatic simulations discussed previously, DFT calculations on CNT-metal contacts only

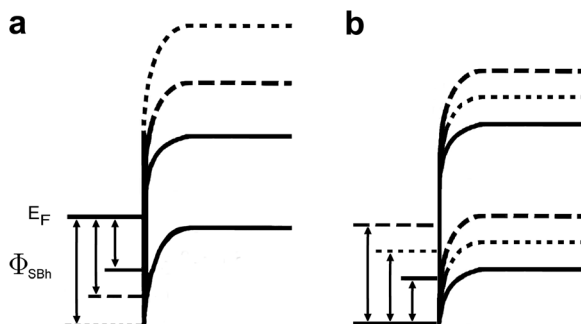


FIG. 7. Schematic band diagrams of the contacts between metals and p-doped CNTs in the absence of Fermi-level pinning. The arrows indicate the Schottky barrier heights for holes. To simplify, the same distance is used between the top of the valence band in the bulk of the CNT and the Fermi level for all CNTs. (a) Contacts to CNTs with large (solid line), intermediate (dashed line) and small (dotted line) diameters. The CNT with the largest diameter has the smallest band gap, and thus, the lowest Schottky barrier. (b) Contacts using metals with high (solid line), intermediate (dotted line), and low (dashed line) work functions. The metal with the highest work function gives the lowest Schottky barrier for holes. Adapted from Z. Chen, J. Appenzeller, J. Knoch, Y. Lin, and P. Avouris, Nano Lett. **5**, 1497 (2005). Copyright © 2005, American Chemical Society.

consider small diameter CNTs and the metals are limited to a few atomic planes due to the large computational resources required.

Some results obtained by DFT calculations suggest that the DOS of a CNT becomes severely distorted when contacted by Ti or Pd.<sup>68,69</sup> Zhu *et al.* have calculated the electrostatic potential and charge distribution for CNTs completely embedded in a Pd crystal. The total number of atoms used in the simulation is only 232 which is still at the limit of what present computational resources can handle. The electrostatic potential profiles through different cross sections of the structure show regions between C and Pd atoms without any potential barrier present (Figure 8). More interestingly, the DOS of the embedded CNT changes dramatically compared to an isolated CNT and its band gap becomes filled with interface states. This results in the CNT no longer being semiconducting once it is embedded in the Pd metal. Meng *et al.* obtained a similar result on planar Ti contacts to CNTs while for an Al contact the CNT retains its semiconducting character (Figure 9).<sup>69</sup>

These results are intriguing since they imply that any Schottky barrier present would be between a metallic-like and semiconducting segment in the same CNT instead of

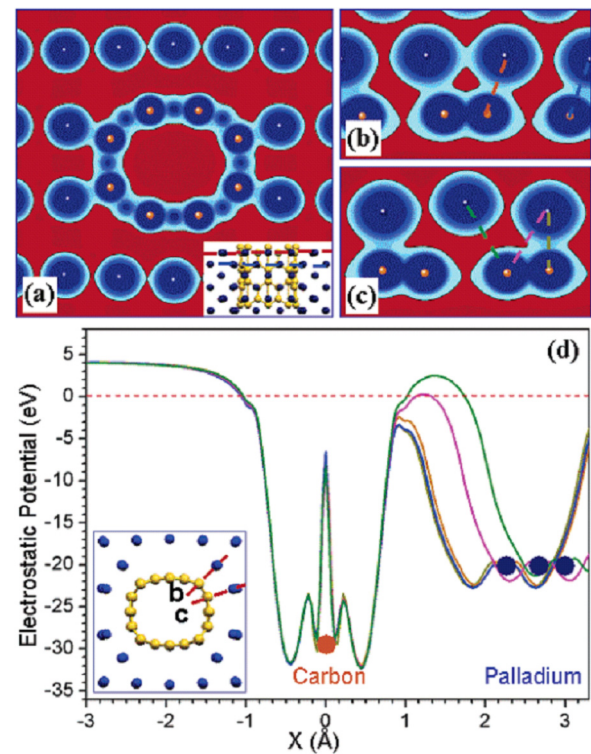


FIG. 8. (Color online) Self-consistent electrostatic potential for a Pd-covered (8,0) nanotube: (a) contours of constant potential plotted in a cross section, indicated by the red line in the inset. In (b) and (c), the potential contours on two different cross sections are shown, which are indicated by lines in the inset of (d), with corresponding labels. The electrostatic potential is negative close to the nuclei and positive inbetween with respect to the Fermi level. (d) The electrostatic potential along five directions passing through C and Pd atoms near the contact region, and extending from the center of the nanotube ( $x = -3 \text{ \AA}$ ) to well within the metal region ( $x = 3 \text{ \AA}$ ); the colors of the curves correspond to the colors of the dashed lines indicating those directions in panels b and c; the red dashed line indicates the Fermi level. Reprinted with permission from W. Zhu and E. Kaxiras, Nano Lett. **6**, 1415 (2006). Copyright © 2006, American Chemical Society.

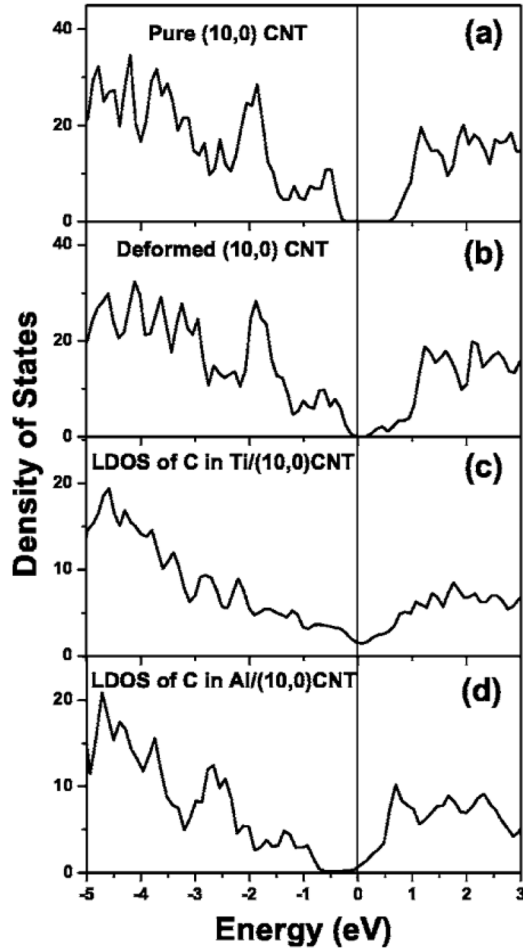


FIG. 9. (a) DOS of an isolated (10,0) CNT. (b) DOS of an isolated (10,0) CNT with the same atomic structure as a CNT adsorbed on a Ti(0001) surface. For (a) and (b), the Fermi level is set to be zero. (c) Projected DOS on C for the Ti-SWCNT system. The vertical line denotes the Fermi level of the Ti-SWCNT system. For this contact, there is a finite DOS at the Fermi level and no band gap. (d) Projected DOS on C for the Al-SWCNT system. The vertical line denotes the Fermi level of the Al-SWCNT system. Reprinted with permission from T. Meng, C. Wang, and S. Wang, J. Appl. Phys. **102**, 013709 (2007). Copyright © 2007, American Institute of Physics.

between the metal contact and the CNT. Such a situation has been modeled by Zhu *et al.* who studied an (8,0) CNT with a segment covered by a ring of Pd atoms that locally modifies the DOS of the CNT.<sup>70</sup> In this study, a Schottky barrier with a height of  $\approx 0.4$  eV for holes was found between the covered and the uncovered part of the CNT.

A few different contact metals have been studied using DFT and it has been found that Al and Au form fewer bonds to CNTs compared to Pd.<sup>71,72</sup> This conclusion is also supported by an experimental study by Zhang *et al.* where different metals were evaporated on suspended CNTs. The results confirm that Pd and Rh wet the CNTs and form a more uniform coating compared to, e.g., Al and Au which aggregate into larger particles.<sup>73</sup>

A comparison between Au and Pd which have similar work functions illustrates that Pd forms a more transparent contact than Au due to the strong electronic coupling to the CNT.<sup>71</sup> The reasons for the stronger coupling are that the change of the DOS in the band gap of the CNT is different

for Au and Pd contacts and that Pd atoms hybridise more strongly with the carbon atoms. A similar result was obtained by Dag *et al.* who compared Mo and Au contacts.<sup>74</sup> Due to poor coupling, the Au contact showed a high potential barrier that electrons have to tunnel through to be injected into the CNT. In contrast, the Mo contact has no tunneling barrier, however, metal-induced gap states pin the Schottky barrier height to  $\approx 0.4$  eV.

Nemec *et al.* have, by comparing Ti and Pd contacts using DFT calculations, concluded that an optimum contact is obtained when there is a weak coupling between the CNT and the metal. Their results also show that Pd atoms hybridise only weakly compared to Ti which explains why Pd is the best choice for low resistance contacts. However, these two conclusions are in strong contrast to other studies that propose that a strong metal-CNT coupling is desirable to obtain a good contact.<sup>71,72,74</sup>

Instead of regarding metal induced gap states to be the origin of the dipole that alters the Schottky barrier height from its ideal value, He *et al.* calculated Schottky barrier heights between CNTs and Pd, Al, and Sc contacts by applying the chemical bond polarisation theory in their DFT calculations.<sup>75</sup> Their calculation shows that due to the different electronegativity of carbon and the contact metals there is a charge redistribution in the bonds with electrons accumulating on the CNT which induces a dipole at the contact (Figure 10). By solving the Poisson equation for the system, the potential shift due to the dipoles is obtained. This shift is then added to the ideal Schottky barrier height calculated from the difference in work function to obtain the actual Schottky barrier height. The extracted Schottky barrier heights are low for Pd (hole barrier) and Sc (electron barrier) and agree well with some of the experimental results.<sup>67,76</sup>

The crystallographic structure of the metal surface is also important with up to 0.2 eV difference in Schottky barrier height between different orientations.<sup>77</sup> It has been

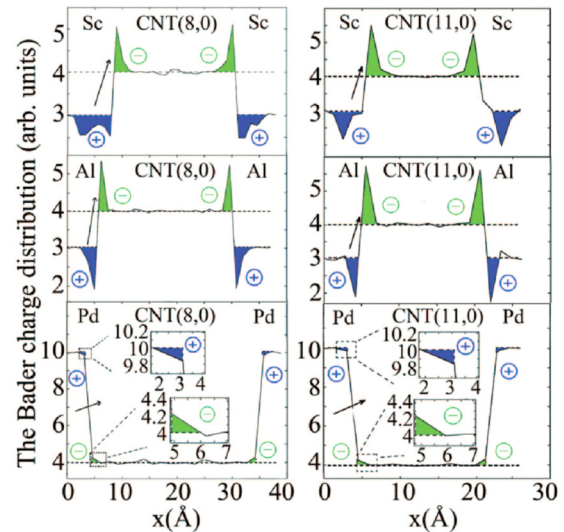


FIG. 10. (Color online) The Bader charge distribution for different CNT-metal contacts along the CNT axis. The arrows show the dipole direction. Reprinted with permission from Y. He, J. Zhang, S. Hou, Y. Wang, and Z. Yu, Appl. Phys. Lett. **94**, 093107 (2009). Copyright © 2009, American Institute of Physics.

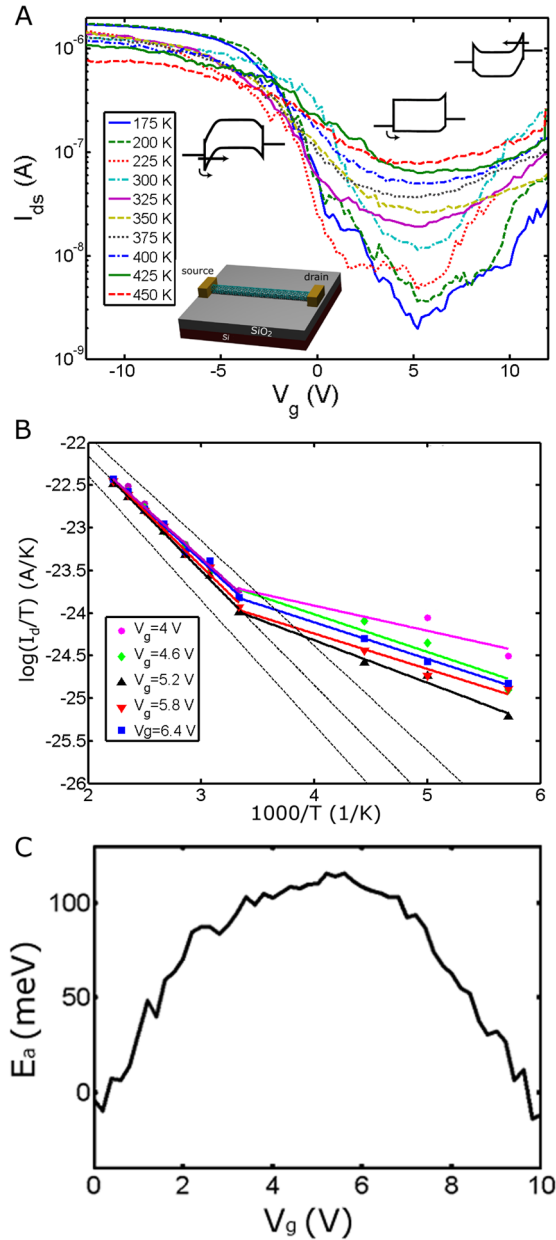


FIG. 11. (Color online) (a) Transfer characteristics of a CNTFET at 10 different temperatures. Schematic band diagrams show hole transport dominated by tunneling for negative  $V_g$ , thermionic emission of holes for intermediate  $V_g$  and electron transport via tunneling at high  $V_g$ . (b) Arrhenius plot with linear fits for five different gate voltages calculated from the transfer characteristics in (a). The dashed lines show the theoretical result for thermionic emission over a barrier with a height of 106, 116, and 126 meV. (c) Activation energy as a function of  $V_g$  calculated from the linear fits for  $T = 300\text{--}450\text{ K}$  in (b). The maximum of 116 meV gives an estimate of the Schottky barrier height. At high and low  $V_g$  the activation energy is reduced due to tunneling. Reprinted with permission from J. Svensson, A. A. Sourab, Y. Tarakanov, D. S. Lee, S. J. Park, S. J. Baek, Y. W. Park, and E. E. B. Campbell, Nanotechnol. **20**, 175204 (2009). Copyright © 2009, Institute of Physics.

concluded that a junction where Al is bonded to the end of a CNT has a considerably higher Schottky barrier compared to a side bonded configuration.<sup>72</sup>

Electrostatic modeling has the drawback that the exact atomic arrangement at the contact is disregarded while DFT modeling can not accurately describe experimental geometries with device dimensions of hundreds of nanometer,

Thus, a modeling scheme that can incorporate both atomic scale potential variations as well as large scale band bending is highly desirable.

## V. SCHOTTKY BARRIER HEIGHT MEASUREMENT TECHNIQUES

The main transport mechanisms in a metal-semiconductor contact are thermionic emission over the Schottky barrier, tunneling through the Schottky barrier and recombination and generation in the space-charge region and in the neutral region. Most semiconductors have a mobility which is high enough so that thermionic emission is the main current limitation and drift-diffusion within the depletion layer can be ignored.<sup>44</sup> If thermionic emission is the only transport mechanism in a Schottky barrier, the electron current from the semiconductor to the metal increases exponentially with voltage at a forward bias but saturates at reverse bias since the barrier for thermionic emission from the metal to the semiconductor is unchanged. However, additional current contributions from tunneling and barrier lowering effects are usually also present. A significant amount of tunneling is only possible if a Schottky barrier is sufficiently thin since the tunneling probability is quickly reduced with increasing barrier thickness. The barrier thickness can be reduced by increasing the electric field close to the interface by, e.g., increasing the doping of the semiconductor. The tunneling current has a weaker temperature dependence compared to thermionic emission which means that it dominates transport at low temperatures.<sup>35</sup>

In contrast to bulk semiconductors, high doping levels are not needed in CNTFETs to achieve a considerable amount of tunneling. This is due to the small diameters of the CNTs that lead to focusing of the electric field from the gate at the contacts.<sup>32</sup> For thin gate oxides and electrodes, the strong field at the contacts makes the Schottky barriers thin enough to allow significant tunneling currents.

The electron current due to thermionic emission in a Schottky barrier between two bulk materials is given by the ideal diode equation

$$I = \overbrace{AA^*T^2e^{-\frac{q\Phi_{SB}}{k_B T}}}^{I_{sat}} e^{\frac{qV}{n k_B T}} \left(1 - e^{-\frac{qV}{k_B T}}\right), \quad (6)$$

where  $A$  is the contact area,  $A^* = 4\pi m^* q k_B^2 / h^3$  the effective Richardson's constant where  $m^*$  is the effective mass,  $V$  the voltage applied to the semiconductor,  $T$  the temperature,  $n$  the ideality factor,  $\Phi_{SB}$  the Schottky barrier height and  $I_{sat}$  the saturation current.<sup>44</sup> A generalisation of Eq. (6) for  $N$ -dimensional materials gives a temperature dependence of  $T^{(N+1)/2}$  and a Richardson's constant of  $A^* = 2^{(N+1)/2} \pi^{(N-1)/2} m^{*(N-1)/2} q k_B^{(N+1)/2} h^{-N}$  due to the different DOS in different dimensions.<sup>78</sup> The ideality factor  $n = (1 - \partial\Phi_{SB}/\partial V)^{-1}$  which describes the dependence of the barrier height on the applied voltage includes barrier lowering effects such as image force lowering, and voltage drops over interfacial layers as well as tunneling. In the ideal case with  $n = 1$  there are no mechanisms that lower the barrier and the current saturates at  $I_{sat}$  for a reverse bias larger than a few times  $k_B T$ .

since the reverse thermionic emission current injected into the metal from the semiconductor (second term in the parenthesis in Eq. (6)) vanishes. However, if  $n > 1$  the current at reverse bias increases exponentially with voltage while the current at forward bias is lowered compared to the ideal case. If  $n > 1.2$  the current is not dominated by thermionic emission and Eq. (6) can not be used reliably.

For bulk metal-semiconductor contacts, there are several methods that can be used to measure the Schottky barrier height and the most commonly used are briefly described here. If transport is dominated by thermionic emission and the contact area and the effective Richardson's constant are known, an estimate of an effective Schottky barrier height at zero bias can be obtained directly from the IV characteristics by extrapolating a plot of  $\ln(I/(1 - e^{-qV/k_B T}))$  as a function of applied voltage to  $V=0$  V. However, the electrically active area is difficult to estimate since it may differ considerably from the geometrical area of the contact due to, e.g., diffusion between the materials rendering this simple method inaccurate.<sup>79</sup>

Since the saturation current in Eq. (6) can be rewritten as

$$\log\left(\frac{I_{sat}}{T^2}\right) = \log(AA^*) - \frac{q\Phi_{SBe}}{k_B T}, \quad (7)$$

The IV characteristics measured at different temperatures can be used to extract the Schottky barrier height. By plotting  $\log(I_{sat}/T^2)$  as a function of  $1/T$  in an Arrhenius plot, a slope of  $-q\Phi_{SBe}/k_B$  is obtained and an intersection with the  $y$ -axis at  $T=\infty$  equal to  $\log(AA^*)$ . This so-called activation energy method is beneficial since it alleviates the need of knowing the effective Richardson's constant or the contact area to extract the Schottky barrier height.

Schottky barrier heights can also be extracted from capacitance-voltage (CV) measurements since the depletion region in a Schottky barrier is acting as a parallel-plate capacitor with a decrease in capacitance with increasing reverse bias due to the increase of the depletion width. In a plot of  $1/C^2$  as a function of reverse bias voltage, the intercept with the  $x$ -axis at  $C=\infty$  corresponds to the Schottky barrier height. However, the CV method is unreliable for low barriers due to the large current at reverse bias which prohibits an accurate extraction of the capacitance and it also requires samples with a sufficiently large contact area to obtain a measurable capacitance.

Another method to measure Schottky barrier heights is to exploit the photoelectric effect. As the photon energy of light illuminating a contact is increased above a certain threshold, electrons are sufficiently excited to be emitted over the Schottky barrier. This threshold energy therefore corresponds to the Schottky barrier height.

For CNT-metal contacts, the choice of measurement technique is severely limited. Since neither the physical contact area nor the Richardson's constant is known, extraction of the Schottky barrier height directly from a single current-voltage measurement is not possible. The CV measurement technique is also difficult to apply due to the small contact area giving capacitances on the order of aF, requiring sophisticated measurement setups.<sup>80</sup> Due to these difficulties

the activation energy method is the most commonly used to measure Schottky barrier heights in CNT-metal contacts.<sup>34,36,81–86</sup> Even though scanning photocurrent measurements have been used to image the depletion region in CNT-metal contacts, quantitative estimates of the Schottky barrier heights using the photoelectric effect are still lacking.<sup>87</sup>

## VI. EXPERIMENTAL STUDIES OF CNT-METAL CONTACTS

For CNTFETs, a low Schottky barrier height for either holes or electrons is preferable depending on whether a p or n-type device is desired. A low Schottky barrier enables a high on-current and a low off-current which is crucial for logic applications. In contrast, an increase in the Schottky barrier height for one type of carriers inevitably results in a decrease of the Schottky barrier height for the other, i.e., the Fermi level of the metal becomes positioned closer to the middle of the band gap resulting in ambipolar characteristics with a significant contribution from both hole and electron currents. In addition, for a CNTFET with contacts with non-zero Schottky barrier heights and a thin gate dielectric, an inverse subthreshold slope close to the thermal limit of 60 mV/dec cannot be achieved since it is tunneling and not thermionic emission that limits the current due to the thin Schottky barrier.<sup>88</sup>

### A. Measurements of Schottky barrier heights

A crucial step towards high performance CNTFETs was achieved by Javey *et al.* who were the first to demonstrate that Pd contacts to CNTs with diameter larger than 1.6 nm give ohmic p-type characteristics with on-currents close to the conductance expected for a ballistic one-dimensional system with four conductance channels ( $G=4e/h^2$ ).<sup>13</sup> The high on-current was attributed to the high work function of Pd which also was altered by exposing the devices to hydrogen. After the exposure, the on-current decreased and the transfer characteristics became more ambipolar due to lowering of the Pd work function. It should be noted that care has to be taken when drawing conclusions about the Schottky barrier height based on the on-state current since it can be affected by the increasing number of sub-bands that contribute to transport at increasing gate voltages.<sup>89</sup> However, since higher sub-bands have a higher Schottky barrier their contribution to the current is limited.

The metal work function is not the sole factor that determines the on-state current but the adhesion between the CNT and the metal is also important since a tunneling barrier that limits the current may form in series with a Schottky barrier. Kim *et al.* have demonstrated that the on-state current depends on the diameter of the CNT also for metallic CNTs, a somewhat surprising result considering that there should be no Schottky barrier present between metal contacts and metallic CNTs.<sup>90</sup> The authors attribute the diameter dependence of metallic CNTs to the increase of the chemical reactivity of CNTs with decreasing diameter which may lead to a large perturbation of the electronic structure of the CNTs underneath the contacts. Au and Pt have work functions similar to

Pd but CNTFETs using these metals as contacts still exhibit low on-currents which have been attributed to the weaker adhesion of these metals to CNTs.<sup>73,91</sup> Noshio *et al.* used Pd, Ti, Mg, and Ca to contact CNTs and observed an increase in the on-state current of the hole branch of the transfer characteristics with increasing metal work function.<sup>92</sup> However, Ca contacts for which a zero Schottky barrier height for electrons is expected, due to the low Ca work function of 2.9 eV, exhibited an electron current lower than expected. This indicates that either the work function of the Ca contact is far from that of a clean surface in vacuum, there is an oxide at the metal-CNT interface or there are additional tunneling barriers limiting the current. It is difficult to obtain n-type CNTFETs that have stable electrical properties in air since low-work-function metals oxidise easily, which severely degrades the electrical characteristics. The best n-type CNTFETs fabricated without doping use Sc or Y as contact metals resulting in stable devices with high electron on-currents.<sup>76,93</sup>

In spite of the possibility of the presence of additional tunneling barriers and transport through multiple sub-bands, the on-state current has been used by Chen *et al.* to estimate the Schottky barrier height of CNT-metal contacts for a large set of devices with different CNT diameters and metal work functions.<sup>67</sup> The Schottky barrier height is extracted by comparing the measured on-state currents to simulations which have the Schottky barrier height as a free parameter.<sup>94</sup> The results suggest that the Schottky barrier height is inversely proportional to the CNT diameter (Figure 12). However, in this study the diameters of the electrically characterised CNTFETs were not measured but instead derived from a statistical treatment of data from transmission electron microscope (TEM) images of a different set of CNTs from the same source material. Therefore, the authors make the assumption that the on-state monotonically increases with increasing CNT diameter. The authors also conclude that the Schottky barrier heights are reduced with increasing metal work function for Pd, Ti, and Al contacts but that the Schottky barrier height difference does not correspond to the values expected using the clean metal work functions.

By using a sensitive capacitance bridge, Tseng *et al.* have succeeded in measuring the minuscule capacitance of the depletion region in CNT-metal contacts and, by using numerical simulations, the capacitances are related to specific Schottky barrier heights.<sup>80</sup> Schottky barrier heights obtained for CNTs contacted by Ti, Nb, and Cr exhibit a decrease with increasing work function and the authors therefore conclude that the Fermi level of the metal is not pinned by interface states.

The two methods described above require additional theoretical simulations to extract Schottky barrier heights but except for such indirect measurements of Schottky barrier heights most studies have been performed on single CNT devices. The first direct measurement of the Schottky barrier height in a CNT-metal contact was reported by Martel *et al.* who used the activation energy method to extract electron and hole Schottky barrier heights of 13 and 15 meV, respectively, for TiC-CNT contacts.<sup>35</sup> These Schottky barrier heights were, however, extracted at high negative and posi-

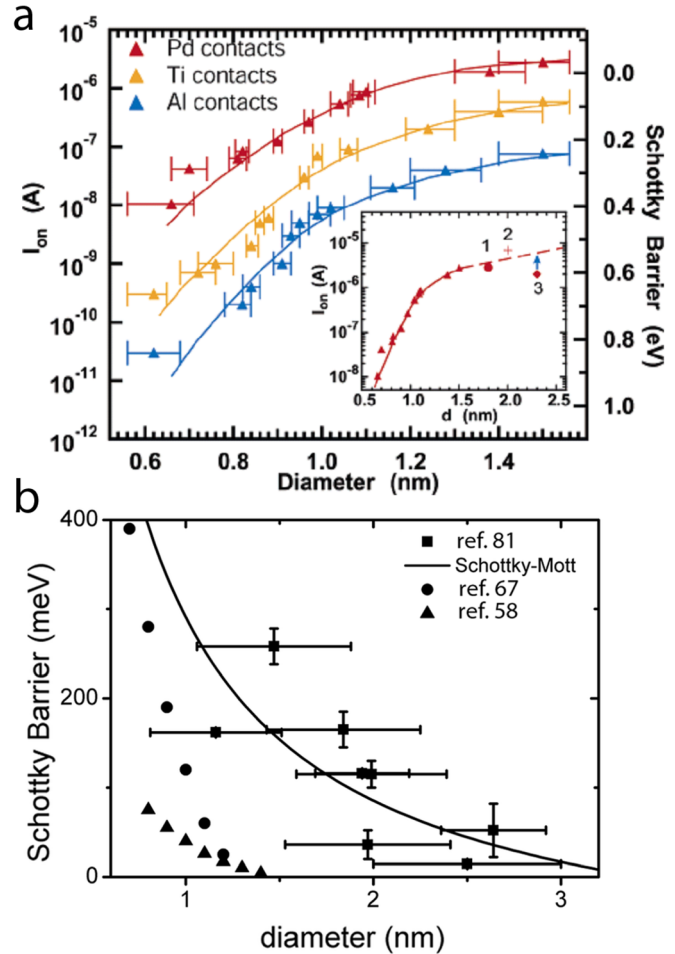


FIG. 12. (Color online) (a) On-current as a function of nanotube diameter for CNTFETs with Pd, Ti, and Al metal contacts. The right axis is the Schottky barrier height extracted from the on-current using theoretical modeling. The inset includes three data points for Pd contacted CNFETs from other publications. Reprinted with permission from Z. Chen, J. Appenzeller, J. Knoch, Y. Lin, and P. Avouris, Nano Lett. **5**, 1497 (2005). Copyright © 2005, American Chemical Society. (b) Schottky barrier heights for holes as a function of CNT diameter in Pd-CNT contacts from activation energy measurements,<sup>81</sup> extracted from on-state currents<sup>67</sup> and theoretical calculations.<sup>58</sup> The solid line corresponds to the dependence expected from the Schottky-Mott relationship (Eq. (3)).

tive gate voltages at which a large band bending resulted in high tunneling currents. Instead of a correct estimate of the Schottky barrier heights, these measurements support the conclusion that tunneling has a large impact on the characteristics of CNTFET devices.

Such high gate voltages have also been used in activation energy measurements to extract low Schottky barriers for Sc (Ref. 76) and Mo (Ref. 85) contacts. However, since these gate voltages allow a considerable amount of tunneling, the extracted values can not be reliably compared to other studies. Appenzeller *et al.* also used the activation energy method to extract the Schottky barrier height for a single Ti contacted CNT.<sup>34</sup> However, instead of measuring only at large gate voltages the activation energy was extracted at a range of voltages (Figure 13). The activation energy was plotted as a function of gate voltage and a Schottky barrier height of 360 meV extracted from the point

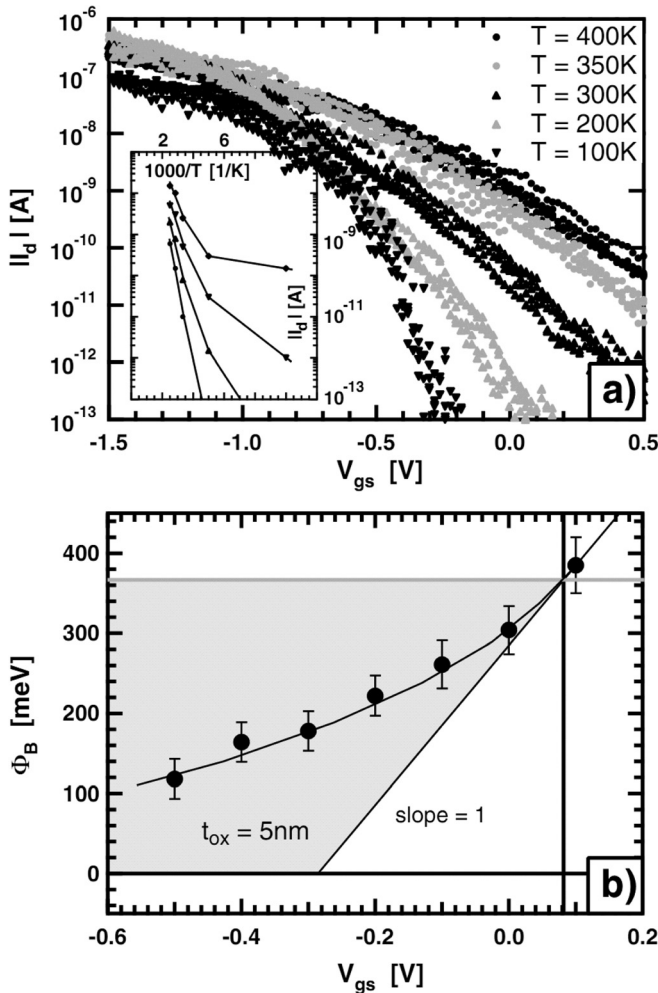


FIG. 13. (a)  $IV_g$  characteristics at different temperatures for a CNTFET with  $t_{ox} = 5$  nm taken at  $V_d = 0.5$  V. The inset displays Arrhenius plots for  $V_g$  values of  $-0.5$ ,  $-0.3$ ,  $-0.1$ , and  $+0.1$  V (from the top to bottom). (b) Schottky barrier height for the same device as a function of  $V_g$ . Reprinted with permission from J. Appenzeller, M. Radosavljević, J. Knoch, and P. Avouris, Phys. Rev. Lett. **92**, 048301 (2004). Copyright © 2004, American Physical Society.

when the slope of this curve was equal to one since this gate voltage should correspond to flat band conditions at one of the contacts, i.e., thermionic emission should dominate. The authors also conclude that for thick gate dielectrics and large diameter CNTs, tunneling is negligible and the thermionic emission limit should be reached for all negative gate voltages. The Schottky barrier height of  $360\text{ meV}$  is close to half the band gap of the CNT indicating that the metal Fermi level is positioned in the middle of the band gap. However, the transfer characteristic of their device is unipolar p-type without any n-branch indicating that the Schottky barrier height for holes should be considerably lower than that for electrons. Any contribution from electron tunneling or thermionic emission is also disregarded in their analysis which is questionable considering the mid-gap Fermi-level position.

A similar measurement approach was used by Chen *et al.* who studied a Cr contacted CNT.<sup>36</sup> After passing a high current through the CNT in vacuum, the device characteristics change from p-type to ambipolar, a change the

authors attributed to the removal of oxygen which p-dopes the CNT. The transfer characteristic was measured at different temperatures and the resulting activation energy as a function of gate voltage showed a maximum corresponding to the Schottky barrier height. It was concluded that the barrier is approximately half the band gap which is expected for a Cr-CNT contact without the influence of Fermi-level pinning. The main difference in the procedure compared to the method used by Appenzeller *et al.*<sup>34</sup> is the position in the activation energy vs gate voltage plot where the Schottky barrier height is extracted. Chen *et al.*<sup>36</sup> argue that for the thick gate dielectric used in their device, tunneling through the Schottky barriers should be negligible at small gate voltages and transport dominated by thermionic emission. However, if tunneling is negligible, it is possible that the measured barrier is not only the Schottky barrier height but has an additional barrier induced by the gate voltage due to the bending of the bands in the bulk of the CNT. Svensson *et al.* who used a similar technique as Chen *et al.*<sup>36</sup> to study the dependence of the Schottky barrier height on the diameter of Pd contacted CNTs observed an activation energy that becomes negative for sufficiently high negative or positive gate voltages (Figure 11).<sup>81</sup> Tunneling dominates transport through CNTFETs at such gate voltages resulting in a small contact resistance, and thus, the temperature dependence of series resistance through the bulk part of the CNT which is opposite to that of thermionic emission give rise to the negative activation energy.

According to Noshio *et al.*, who used Ca as contact metal to create n-type CNTFETs, the activation energy extracted from temperature dependent measurements approaches the true Schottky barrier height for decreasing gate voltage.<sup>95</sup> However, for their unipolar device, where only a n-branch is observable, the activation energy for large negative gate voltages would correspond to the Schottky barrier height plus an additional gate induced barrier.

The three studies that use the activation energy method mentioned above were all performed on single CNTs but there are also a few studies that use this method to characterise the Schottky barriers in devices with multiple CNTs in the channel.<sup>82,96</sup> Even though such studies can give important information about, for example, the impact of adsorbed molecules<sup>82</sup> or doping,<sup>96</sup> the mixture of metallic, semiconducting, and small band gap CNTs of various diameter makes it difficult to draw any conclusions regarding the impact of the metal work function or CNT diameter on the Schottky barrier height.

The studies mentioned above are either focused on single devices with individual CNTs or devices with multiple CNTs in the channel. However, direct measurements of the Schottky barrier height for a larger set of devices is important to gain a more profound understanding of the factors that influence the Schottky barrier height. Svensson *et al.* studied the Schottky barrier height in Pd-CNT contacts for eight CNTs with different diameters using the activation energy method.<sup>81</sup> The Schottky barrier heights were found to be inversely proportional to the diameter as expected due to the decrease in band gap with increasing diameter (Figure 12(b)).

Since Schottky barrier heights in CNT-metal contacts are expected to depend both on CNT diameter and metal work function, it is difficult to distinguish the impact of each of these contributions separately if values from devices with different contact metals and CNTs are compared. To circumvent this problem Perello *et al.* have fabricated CNTFETs with Hf, Cr, Ti and Pd electrodes on the same CNTs.<sup>84</sup> Since the diameter is identical along the CNT, this approach allows for a comparison between different metal work functions. The authors used temperature dependent measurements to extract the activation energy at different gate voltages and extrapolate to zero gate voltage (Figure 14) to exclude any effect from barrier lowering due to tunneling or image force lowering at higher gate voltages and obtain a good estimate of the Schottky barrier height. The authors find that the activation energy decreases exponentially with increasing positive or negative gate voltages. By assuming that the Schottky barrier height is unpinned they also extract the Fermi level position of the CNT using the clean metal work functions of the contacts ( $\Phi_{SB\text{e}} + \Phi_m = E_F$  and  $\Phi_m - \Phi_{SB\text{h}} = E_F$ ). Due to a small region of negative transconductance in the transfer characteristic for Hf contacts at high source-drain bias the authors conclude that band-to-band tunneling is important for this metal species. Moreover Hf, which has the lowest work function of the metals and is therefore expected to have a dominant n-type behavior, exhibits a high Schottky barrier height for electrons and a dominant hole p-branch with only

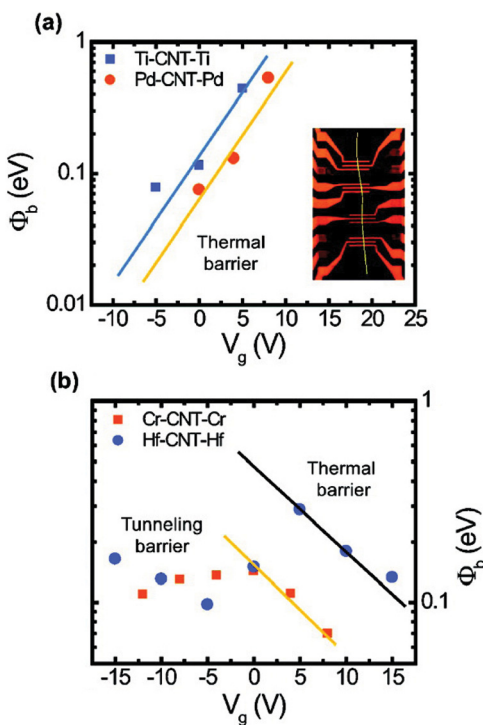


FIG. 14. (Color online) (a) Schottky barriers extracted using activation energy measurements: Ti (square) and Pd (circle) barrier heights as a function of gate voltage. Inset: Optical image of the device layout. The solid line denotes the location of the single CNT used for all the measurements with four different metal electrodes. (b) Schottky barrier heights for low-work-function metals Cr (square) and Hf (circle). The solid lines are least-squares fits to the data. Reprinted with permission from D. J. Perello, S. ChuLim, S. J. Chae, I. Lee, M. J. Kim, Y. H. Lee, and M. Yun, ACS Nano 4, 3103 (2010). Copyright © 2010, American Chemical Society.

a small electron current at positive gate voltages. These somewhat surprising results lead the authors to introduce a new model for Schottky barriers in CNT-metal contacts based on the formation of a surface inversion layer close to the contact in the case of a low-work-function metal (Figure 15). Since low-work-function metals are very reactive it is expected that a thin oxide layer is formed at the edge of the contact. This layer results in electron transfer from the CNT to the metal, and thus, a p-type region is present in series with the n-type part of the CNT underneath the unoxidised metal. The carriers entering the CNT, thus, either have to pass through both regions or be injected through the oxidised part of the metal. This description of the CNT-metal contact is used to explain the surprisingly high electron Schottky barrier for Hf and the observed band-to-band tunneling. The authors conclude that to achieve air-stable n-type CNTFETs, a low work function metal with a weak surface dipole should preferably be used.

That the segment of the CNT underneath the metal electrode and not only the electrode edge is important for transport is also supported by a study by Franklin *et al.*, who found a rapidly increasing contact resistance for contact lengths below 100 nm.<sup>97</sup>

To summarise the experimental results, the Schottky barrier heights from the activation energy studies<sup>34,36,81,83,84,86</sup> where the CNT diameter was determined

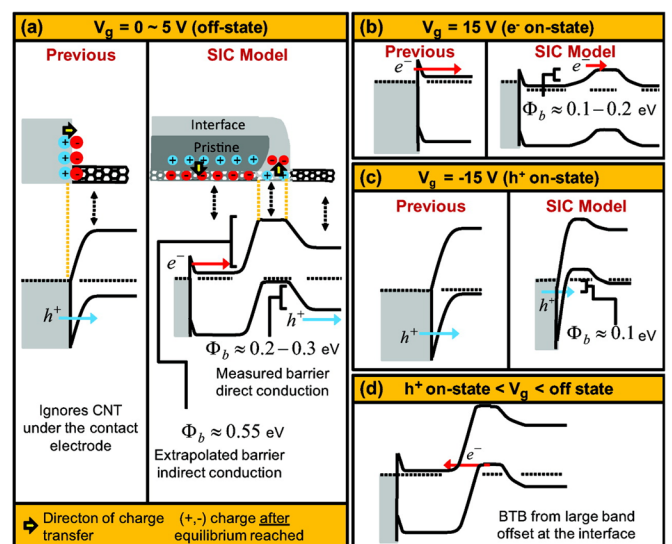


FIG. 15. (Color online) (a) Top panels show the charge transfer between CNT and Hf (low-work-function metal) with exposure to oxygen. The bottom panels show a comparison of a typical band diagram of a surface dipole layer model and a surface inversion channel (SIC) model. In the surface dipole layer model, band bending occurs due to the formation of a dipole layer and holes tunnel through the regular Schottky barrier. In the SIC model, three distinct CNT regions are formed: metal-covered CNT, CNT inversion layer, and intrinsic channel. (b) Band diagram of electron conducting on-state at  $V_g = 15$  V. An electron barrier between the metal-covered section of the CNT and the inversion region dominates conduction. (c) Band diagram of hole conducting on-state at  $V_g = -15$  V. Tunneling dominates and transport is governed by direct injection of holes from the metal. (d) The band diagram at intermediate gate bias shows negative transconductance due to band-to-band tunneling resulting from a large band offset at the interface. Reprinted with permission from D. J. Perello, S. ChuLim, S. J. Chae, I. Lee, M. J. Kim, Y. H. Lee, and M. Yun, ACS Nano 4, 3103 (2010). Copyright © 2010, American Chemical Society.

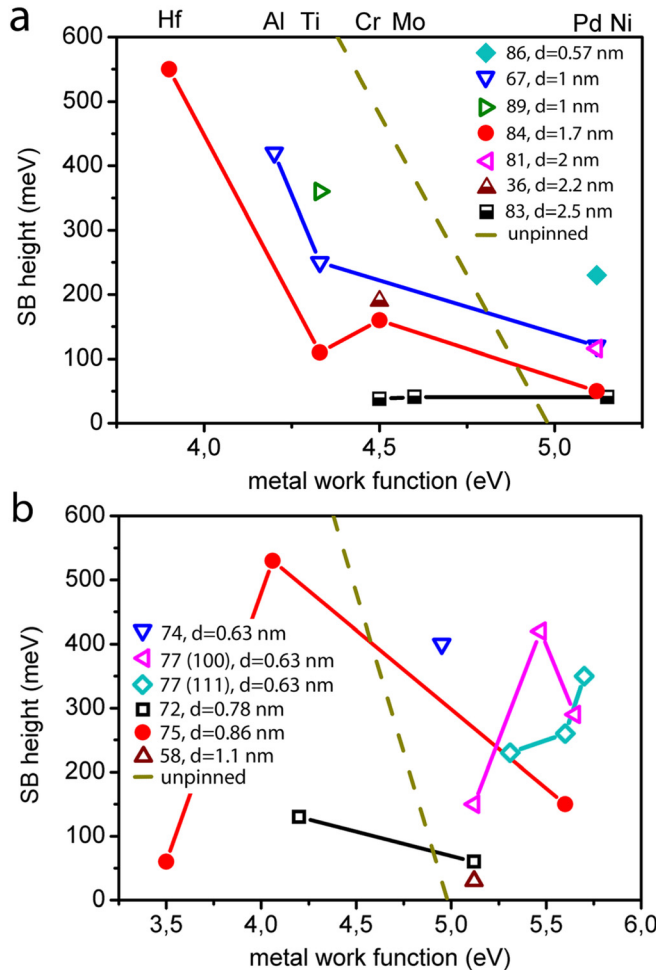


FIG. 16. (Color online) Schottky barrier height as a function of metal work function for CNTs of different diameter. The closed and open symbols correspond to electron and hole barriers, respectively, and the half filled symbols correspond to measurements where the barrier type is unknown. The corresponding reference number is in the legend. The dashed line illustrates the expected hole Schottky barrier height for a CNT-metal contact which is unaffected by Fermi level pinning assuming a CNT work function of 4.58 eV and a diameter of 1 nm.<sup>99</sup> (a) Experimental results. All data except those from Chen *et al.*<sup>67</sup> have been obtained using the activation energy method. The CNT diameters have been measured using AFM except for Chen *et al.*<sup>67</sup> and Appenzeller *et al.*<sup>34</sup> where only the diameters of other CNTs from the same production source were measured. (b) Theoretical results. The metal work functions for the crystal orientations used in the calculation have been used if available, otherwise work functions for polycrystalline surfaces have been used.

are plotted as a function of the metal work function<sup>98</sup> in Figure 16. In addition, results from Chen *et al.* who extracted the Schottky barrier height from the on-current for three different metals are also included.<sup>67</sup> Due to the large range of diameters between 0.57 and 2.5 nm it is difficult to quantitatively compare the different sets of data but some interesting observations can at least be made. The smallest diameter CNT with  $d = 0.57$  nm and a Pd contact, from Jejurikar *et al.*, has a barrier height of 230 meV. Interestingly, this device exhibits n-type characteristics<sup>86</sup> in spite of the high-work-function metal used. This observation is due to the work function of CNTs increasing with decreasing diameter due to hybridisation.<sup>99</sup> For sufficiently small diameters, the CNT work function becomes larger than that of Pd resulting

in an electron Schottky barrier which is smaller than the hole Schottky barrier. A similar observation of n-type characteristics for a high-work-function metal has been made by Moon *et al.*<sup>100</sup> However, they attributed the n-type characteristics to the high-energy deposition method used for their Co contacts, which results in strong chemical bonds between metal and CNT pinning the Fermi level of the metal close to the middle of the CNT band gap.

The results from Perello *et al.* who fabricated Cr, Mo and Ni contacts on a single CNT give very low and almost identical barriers for all metals indicating that the metal work function has little impact on the Schottky barrier height in this experiment. However, since the CNT has a large diameter of 2.5 nm, and thus, a band gap of only  $E_g = 0.3$  eV it is possible that the measured activation energies are actually due to potential barriers in the bulk of the CNT and not Schottky barriers at the contacts.<sup>101</sup>

The two other studies that have reported measurements with different metals on CNTs with identical diameters show a decrease in Schottky barrier height with increasing work function.<sup>67,84</sup> However, the slope of this decrease is less than what is expected from the Schottky-Mott description (Eq. (2)) of a barrier unaffected by Fermi level pinning (dashed line in Figure 16(a)). For metal work functions smaller than that of CNTs, the electron Schottky barrier height is expected to dominate transport and the measured Schottky barrier to decrease with decreasing metal work function. However, the results in Figure 16(a) show a high Schottky barrier also for low work function metals such as Hf and Al.

It should be noted that the values of the metal work function used in Figure 16 are those of a clean polycrystalline surface in vacuum and that differences of 100 s of meV for different crystal orientations have been observed.<sup>102</sup> Even though most of the measurements are performed in vacuum or in an inert atmosphere, there could still be adsorbents present that alter the work function considerably. For example, exposure to air is known to reduce the work function of Au by up to 0.6 eV compared to a clean surface in vacuum due to hydrocarbon adsorption<sup>103</sup> and oxidation of Al can increase its work function by up to 1 eV.<sup>104</sup> It has also been demonstrated that alkanethiol, S and O<sub>2</sub> adsorbed at the interface between a CNT and an Au surface results in an interface dipole which alters the band line-up between metal and CNT and therefore also the Schottky barrier height.<sup>105</sup> Measurements of the work function of CNTs also exhibit a wide range of values between 4.8 and 5.05 eV (Refs. 106–108) while theoretical calculations suggest a strong diameter dependence of the work function with values between 4.51 and 5.17 eV for a diameter range of 0.41–1.57 nm.<sup>99</sup>

A compilation of the data from the theoretical simulations described in the previous chapter shows very large scatter which suggests that there is little correlation between the metal work function and the Schottky barrier height (Figure 16(b)).

## B. Imaging of depletion region

The activation energy measurements do not yield any information about the spatial extent of the depletion width in

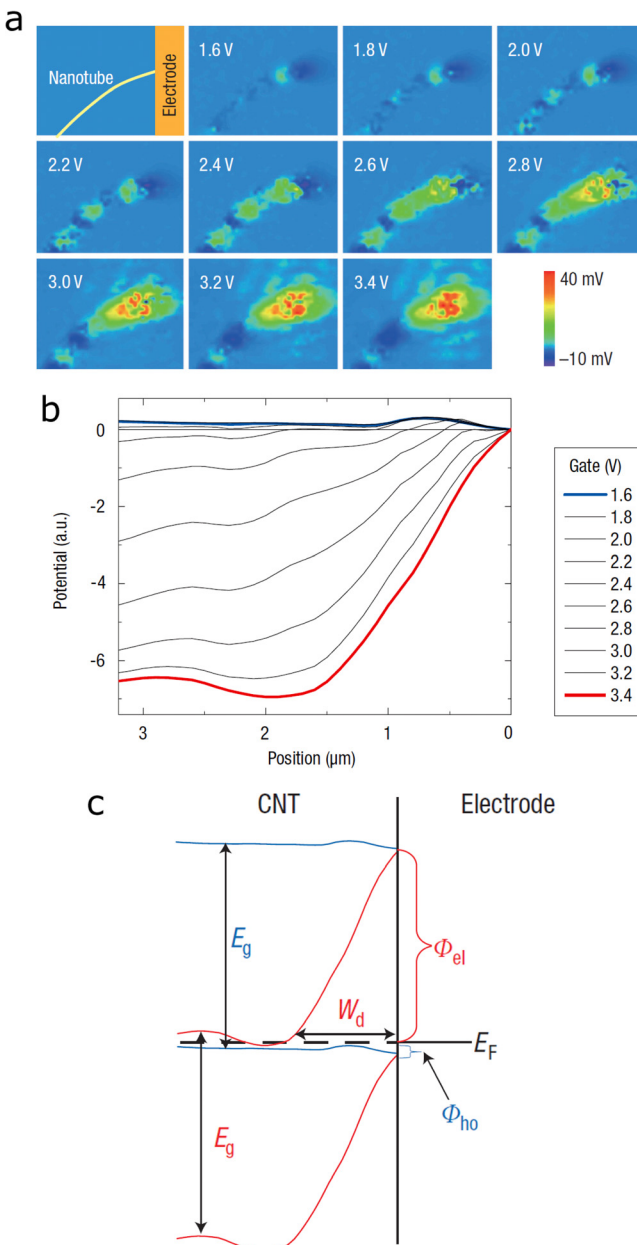


FIG. 17. (Color online) Open-circuit photovoltage microscopy of the contact region in a Pd-CNT contact. (a) Open circuit voltage images of the Schottky-barrier region at different gate voltages during the transition from p-type to n-type conduction in the transistor off state. The first panel is a schematic of the device. (b) Integrated open circuit voltage signal along the length of the CNT. The metal contact is located at the origin of the position scale, and the potential was fixed there for all gate voltages. (c) Schematic of the band bending for the two threshold voltages for hole and electron conduction at  $V_g = 1.6$  and  $3.4 \text{ V}$ . The Schottky barrier heights for electrons and holes ( $\Phi_{el}$  and  $\Phi_{ho}$ ) and the depletion width at the threshold for electron conduction ( $W_d$ ) are indicated. Reprinted with permission from M. Freitag, J. C. Tsang, A. Bol, D. Yuan, J. Liu, and P. Avouris, Nano Lett. 7, 2037 (2007). Copyright © 2007, American Chemical Society.

CNT-metal contacts. Therefore, the depletion regions in CNT-metal contacts have been imaged using photocurrent and photovoltage measurements<sup>87</sup> as well as by scanned gate microscopy.<sup>109</sup>

In the scanned gate microscopy experiments, it was observed that a biased AFM tip scanned over a CNTFET has a stronger gating effect when the tip is in the vicinity of one

of the contacts implying that a barrier is present there. However, the spatial resolution of this technique is limited due to the finite distance between the tip and the CNT but an upper limit for the depletion width of 50 nm could still be deduced.

Freitag *et al.* used photovoltage and photocurrent measurements to image the depletion region by irradiating the CNT-metal contact with a laser and measuring the current or voltage. The electron-hole pairs that are generated by the incoming photons are separated by the internal electric field in the depletion region which gives rise to a strong signal as the laser spot is positioned close to the contact. The results illustrate that the depletion width can extend up to  $1.5 \mu\text{m}$  from the edge of the contact into the CNT at a gate voltage corresponding to the off-state of the device and decrease below 500 nm in the on-state (Figure 17). Even though a quantitative value of the Schottky barrier height could not be deduced from this experiment it was clear that the hole barrier is considerably higher than the electron barrier in a Pd contacted device.

## VII. CONCLUSIONS

From an engineering perspective, it is possible to obtain good contacts to CNTs by choosing a metal with high or low work function for p or n type CNTFETs, respectively, and by using CNTs with sufficiently large diameter. However, as is evident from the large discrepancies in both theoretical and experimental results, there is still a lack of understanding of the details of the Schottky barrier formation and the influence of interface dipoles. Theoretical modeling gives a wealth of different results predicting either no influence of interface states,<sup>57,58</sup> a high sensitivity to the microscopic bonding configuration and crystal orientation<sup>72,77</sup> and even that a semiconducting CNT underneath a contact becomes metallic-like due to the filling of the band gap with interface states.<sup>68,69</sup> The theoretical results are usually difficult to compare to experimental data due to the idealised geometry used in, e.g., DFT calculations and that important effects from, e.g., adsorbents are not considered. Also, the experimental results reported in the literature usually lack measurements of metal and CNT work functions and have a high uncertainty in diameter determination.

The poor understanding of the most important factors that affect Schottky barrier formation in metal-CNT contacts stems from the difficulty in using many of the techniques available for bulk materials to perform measurements on Schottky barriers in nanoscale contacts. For bulk contacts, several measurement techniques are usually employed on the same sample to validate that the extracted Schottky barrier heights are correct. However, for CNT-metal contacts, the activation energy method that utilises temperature dependent electrical characterisation is presently the only method to obtain quantitative Schottky barrier heights without the need for theoretical modeling. To ensure that measured Schottky barrier heights are correct, a second method for nanoscale contacts should be developed. Ideally, a combination of activation energy, capacitive<sup>80</sup> and optical<sup>87</sup> measurement techniques should be used to study the Schottky barriers on different metals deposited on a single CNT.<sup>84</sup> In combination

with Kelvin probe microscopy<sup>105</sup> to measure the work function of the different metals on the device instead of relying on tabulated values for ideal surfaces, such a study would yield a wealth of important information on the physics of Schottky barrier formation in nanoscale contacts and the influence of interface states on the Schottky barrier height.

## ACKNOWLEDGMENTS

Financial support from Vetenskapsrådet (VR), SSF, and the WCU program of the MEST (R31-2008-000-10057-0), is gratefully acknowledged.

- <sup>1</sup>G. E. Moore, *Electronics* **38**, 114 (1965).
- <sup>2</sup>G. E. Moore, IEEE IEDM Tech. Digest **21**, 11 (1975).
- <sup>3</sup>S. Iijima, *Nature (London)* **354**, 56 (1991).
- <sup>4</sup>K. S. Novoselov, A. K. Geim, S. V. Morozov, D. Jiang, Y. Zhang, S. V. Dubonos, I. V. Grigorieva, and A. A. Firsov, *Science* **306**, 666 (2004).
- <sup>5</sup>M. Y. Han, B. Özyilmaz, Y. Zhang, and P. Kim, *Phys. Rev. Lett.* **98**, 206805 (2007).
- <sup>6</sup>X. Li, X. Wang, L. Zhang, S. Lee, and H. Dai, *Science* **319**, 1229 (2008).
- <sup>7</sup>J. Bai, X. Zhong, S. Jiang, Y. Huang, and X. Duan, *Nat. Nanotechnol.* **5**, 190 (2010).
- <sup>8</sup>D. C. Elias, R. R. Nair, T. M. G. Mohiuddin, S. V. Morozov, P. Blake, M. P. Halsall, A. C. Ferrari, D. W. Boukhvalov, M. I. Katsnelson, A. K. Geim, and K. S. Novoselov, *Science* **323**, 610 (2009).
- <sup>9</sup>X. Wu, M. Sprinkle, X. Li, F. Ming, C. Berger, and W. A. de Heer, *Phys. Rev. Lett.* **101**, 026801 (2008).
- <sup>10</sup>F. Schwierz, *Nat. Nanotechnol.* **5**, 487 (2010).
- <sup>11</sup>T. Duerkop, S. A. Getty, E. Cobas, and M. S. Fuhrer, *Nano Lett.* **4**, 35 (2004).
- <sup>12</sup>Z. Y. Zhang, S. Wang, L. Ding, X. L. Liang, H. L. Xu, J. Shen, Q. Chen, R. L. Cui, Y. Li, and L. M. Peng, *Appl. Phys. Lett.* **92**, 133117 (2008).
- <sup>13</sup>A. Javey, J. Guo, Q. Wang, M. Lundstrom, and H. Dai, *Nature (London)* **424**, 654 (2003).
- <sup>14</sup>S. Iijima and T. Ichihashi, *Nature (London)* **363**, 603 (1993).
- <sup>15</sup>X. Wang, Q. Li, J. Xie, Z. Jin, J. Wang, Y. Li, K. Jiang, and S. Fan, *Nano Lett.* **9**, 3137 (2009).
- <sup>16</sup>X. Zhou, "Carbon nanotube transistors, sensors, and beyond," Ph.D. dissertation (Cornell University, 2008).
- <sup>17</sup>R. Saito, M. Fujita, G. Dresselhaus, and M. S. Dresselhaus, *Phys. Rev. B* **46**, 1804 (1992).
- <sup>18</sup>J. W. G. Wilder, L. C. Venema, A. G. Rinzler, R. E. Smalley, and C. Dekker, *Nature (London)* **391**, 59 (1998).
- <sup>19</sup>R. B. Weisman and S. M. Bachilo, *Nano Lett.* **3**, 1235 (2003).
- <sup>20</sup>S. Ilani and P. L. McEuen, *Annu. Rev. Condens. Matter Phys.* **1**, 1 (2010).
- <sup>21</sup>E. Minot, "Tuning the band structure of carbon nanotubes," Ph.D. dissertation (Cornell University, 2004).
- <sup>22</sup>C. L. Kane and E. J. Mele, *Phys. Rev. Lett.* **78**, 1932 (1997).
- <sup>23</sup>E. Minot, Y. Yaish, V. Sazonova, J. Park, M. Brink, and P. McEuen, *Phys. Rev. Lett.* **90**, 156401 (2003).
- <sup>24</sup>M. Huang, Y. Wu, B. Chandra, H. Yan, Y. Shan, T. F. Heinz, and J. Hone, *Phys. Rev. Lett.* **100**, 136803 (2008).
- <sup>25</sup>A. Javey, J. Guo, M. Paulsson, Q. Wang, D. Mann, M. Lundstrom, and H. Dai, *Phys. Rev. Lett.* **92**, 106804 (2004).
- <sup>26</sup>J.-Y. Park, S. Rosenblatt, Y. Yaish, V. Sazonova, H. Uestuenel, S. Braig, T. A. Arias, P. W. Brouwer, and P. L. McEuen, *Nano Lett.* **4**, 517 (2004).
- <sup>27</sup>R. V. Seidel, A. P. Graham, J. Kretz, B. Rajasekharan, G. S. Duesberg, M. Liebau, E. Unger, F. Kreupl, and W. Hoenlein, *Nano Lett.* **5**, 147 (2005).
- <sup>28</sup>A. Javey, H. Kim, M. Brink, Q. Wang, A. Ural, J. Guo, P. McIntyre, P. McEuen, M. Lundstrom, and H. Dai, *Nature Mater.* **1**, 241 (2002).
- <sup>29</sup>S. J. Tans, R. M. Verschueren, and C. Dekker, *Nature (London)* **393**, 49 (1998).
- <sup>30</sup>R. Martel, T. Schmidt, H. R. Shea, T. Hertel, and P. Avouris, *Appl. Phys. Lett.* **73**, 2447 (1998).
- <sup>31</sup>C. Zhou, J. Kong, and H. Dai, *Appl. Phys. Lett.* **76**, 1597 (2000).
- <sup>32</sup>S. Heinze, J. Tersoff, R. Martel, V. Derycke, J. Appenzeller, and P. Avouris, *Phys. Rev. Lett.* **89**, 106801 (2002).
- <sup>33</sup>V. Derycke, R. Martel, J. Appenzeller, and P. Avouris, *Appl. Phys. Lett.* **80**, 2773 (2002).
- <sup>34</sup>J. Appenzeller, M. Radosavljević, J. Knob, and P. Avouris, *Phys. Rev. Lett.* **92**, 048301 (2004).
- <sup>35</sup>R. Martel, V. Derycke, C. Lavoie, J. Appenzeller, K. Chan, J. Tersoff, and P. Avouris, *Phys. Rev. Lett.* **87**, 256805 (2001).
- <sup>36</sup>Y. Chen and M. S. Fuhrer, *Nano Lett.* **6**, 2158 (2006).
- <sup>37</sup>C. M. Aguirre, P. L. Levesque, M. Paillet, F. Lapointe, B. C. St-Antoine, P. Desjardins, and R. Martel, *Adv. Mater.* **21**, 3087 (2009).
- <sup>38</sup>J.-C. Charlier, X. Blase, and S. Roche, *Rev. Mod. Phys.* **79**, 677 (2007).
- <sup>39</sup>P. Avouris, Z. Chen, and V. Perebeinos, *Nat. Nanotechnol.* **2**, 605 (2007).
- <sup>40</sup>P. Avouris, *Phys. Today* **62**, 34 (2009).
- <sup>41</sup>A. Javey and J. Kong, *Carbon Nanotube Electronics* (Springer, New York, 2009).
- <sup>42</sup>C. Rutherglen, D. Jain, and P. Burke, *Nat. Nanotechnol.* **4**, 811 (2009).
- <sup>43</sup>E. Cobas and M. S. Fuhrer, *Appl. Phys. Lett.* **93**, 043120 (2008).
- <sup>44</sup>E. H. Rhoderick and R. H. Williams, *Metal-Semiconductor Contacts*, 2nd ed. (Clarendon Press, 1988).
- <sup>45</sup>W. Monch, *Rep. Prog. Phys.* **53**, 221 (1990).
- <sup>46</sup>W. Schottky, *Phys. Z.* **41**, 570 (1940).
- <sup>47</sup>N. F. Mott, *Proc. Cambridge Philos. Soc.* **34**, 568 (1938).
- <sup>48</sup>A. Cowley and S. Sze, *J. Appl. Phys.* **36**, 3212 (1965).
- <sup>49</sup>V. Heine, *Phys. Rev.* **138**, 1689 (1965).
- <sup>50</sup>S. G. Louie and M. L. Cohen, *Phys. Rev. B* **13**, 2461 (1976).
- <sup>51</sup>J. Tersoff, *Phys. Rev. Lett.* **52**, 465 (1984).
- <sup>52</sup>R. T. Tung, *Phys. Rev. Lett.* **84**, 6078 (2000).
- <sup>53</sup>R. T. Tung, *Phys. Rev. B* **64**, 205310 (2001).
- <sup>54</sup>J. Piscator, "Influence of electron charge states in nanoelectronic building blocks," Ph.D. dissertation, (Chalmers University of Technology, 2009).
- <sup>55</sup>G. Song, M. Y. Ali, and M. Tao, *IEEE Electron. Device Lett.* **28**, 71 (2007).
- <sup>56</sup>A. Vilan, A. Shanzer, and D. Cahen, *Nature (London)* **404**, 166 (2000).
- <sup>57</sup>F. Léonard and J. Tersoff, *Phys. Rev. Lett.* **84**, 4693 (2000).
- <sup>58</sup>F. Léonard and A. A. Talin, *Phys. Rev. Lett.* **97**, 026804 (2006).
- <sup>59</sup>A. A. Odintsov, *Phys. Rev. Lett.* **85**, 150 (2000).
- <sup>60</sup>T. Nakanishi, A. Bachtold, and C. Dekker, *Phys. Rev. B* **66**, 073307 (2002).
- <sup>61</sup>D. Jiménez, X. Cartoixà, E. Miranda, J. S. né, F. A. Chaves, and S. Roche, *Nanotechnology* **18**, 025201 (2007).
- <sup>62</sup>Y. Xue and M. A. Ratner, *Phys. Rev. B* **70**, 205416 (2004).
- <sup>63</sup>A. Maiti and A. Ricca, *Chem. Phys. Lett.* **395**, 7 (2004).
- <sup>64</sup>J. A. Rodriguez-Manzo, F. Banhart, M. Terrones, H. Terrones, N. Grobert, P. M. Ajayan, B. G. Sumpter, V. Meunier, M. Wang, Y. Bando, and D. Golberg, *Proc. Natl. Acad. Sci. USA* **106**, 4591 (2009).
- <sup>65</sup>C. Berger, Y. Yi, J. Gezo, P. Poncharal, and W. A. de Heer, *New J. Phys.* **5**, 158 (2003).
- <sup>66</sup>J. J. Palacios, A. J. Pérez-Jiménez, E. Louis, E. SanFabián, and J. A. Vergés, *Phys. Rev. Lett.* **90**, 106801 (2003).
- <sup>67</sup>Z. Chen, J. Appenzeller, J. Knob, Y. Lin, and P. Avouris, *Nano Lett.* **5**, 1497 (2005).
- <sup>68</sup>W. Zhu and E. Kaxiras, *Nano Lett.* **6**, 1415 (2006).
- <sup>69</sup>T. Meng, C. Wang, and S. Wang, *J. Appl. Phys.* **102**, 013709 (2007).
- <sup>70</sup>W. Zhu and E. Kaxiras, *Appl. Phys. Lett.* **89**, 243107 (2006b).
- <sup>71</sup>J. J. Palacios, P. Tarakeshwar, and D. M. Kim, *Phys. Rev. B* **77**, 113403 (2008).
- <sup>72</sup>V. Vitale, A. Curioni, and W. Andreoni, *J. Am. Chem. Soc.* **130**, 5848 (2008).
- <sup>73</sup>Y. Zhang, N. Franklin, R. Chen, and H. Dai, *Chem. Phys. Lett.* **331**, 35 (2000).
- <sup>74</sup>S. Dag, O. Güleren, S. Ciraci, and T. Yıldırım, *Appl. Phys. Lett.* **83**, 3180 (2003).
- <sup>75</sup>Y. He, J. Zhang, S. Hou, Y. Wang, and Z. Yu, *Appl. Phys. Lett.* **94**, 093107 (2009).
- <sup>76</sup>Z. Zhang, X. Liang, S. Wang, K. Yao, Y. Hu, Y. Zhu, Q. Chen, W. Zhou, Y. Li, Y. Yao, J. Zhang, and L. M. Peng, *Nano Lett.* **7**, 3603 (2007).
- <sup>77</sup>B. Shan and K. Cho, *Phys. Rev. B* **70**, 233405 (2004).
- <sup>78</sup>M. F. ODwyer, R. A. Lewis, and C. Zhang, *Microelectron. J.* **39**, 597 (2008).
- <sup>79</sup>S. M. Sze and K. K. Ng, *Physics of Semiconductor Devices*, 3rd ed. (Wiley, 2007).
- <sup>80</sup>Y.-C. Tseng and J. Bokor, *Appl. Phys. Lett.* **96**, 013103 (2010).
- <sup>81</sup>J. Svensson, A. A. Sourab, Y. Tarakanov, D. S. Lee, S. J. Park, S. J. Baek, Y. W. Park, and E. E. B. Campbell, *Nanotechnol.* **20**, 175204 (2009).

- <sup>82</sup>C. W. Lee, K. Zhang, H. Tantang, A. Lohani, S. G. Mhaisalkar, L.-J. Li, T. Nagahiro, K. Tamada, and Y. Chen, *Appl. Phys. Lett.* **91**, 103515 (2007).
- <sup>83</sup>D. Perello, D. J. Bae, M. J. Kim, D. K. Cha, S. Y. Jeong, B. R. Kang, W. J. Yu, Y. H. Lee, and M. Yun, *IEEE Trans. Nanotechnol.* **8**, 355 (2009).
- <sup>84</sup>D. J. Perello, S. ChuLim, S. J. Chae, I. Lee, M. J. Kim, Y. H. Lee, and M. Yun, *ACS Nano* **4**, 3103 (2010).
- <sup>85</sup>N. Inami, M. A. Mohamed, E. Shikoh, and A. Fujiwara, *Appl. Phys. Lett.* **92** (2008).
- <sup>86</sup>S. Jejurikar, D. Casterman, P. B. Pillai, O. Petrenko, M. M. D. Souza, A. Tahraoui, C. Durkan, and W. I. Milne, *Nanotechnol.* **21**, 215202 (2010).
- <sup>87</sup>M. Freitag, J. C. Tsang, A. Bol, D. Yuan, J. Liu, and P. Avouris, *Nano Lett.* **7**, 2037 (2007).
- <sup>88</sup>J. Appenzeller, J. Knoch, V. Derycke, R. Martel, S. Wind, and P. Avouris, *Phys. Rev. Lett.* **89**, 126801 (2002).
- <sup>89</sup>J. Appenzeller, J. Knoch, M. Radosavljević, and P. Avouris, *Phys. Rev. Lett.* **92**, 226802 (2004).
- <sup>90</sup>W. Kim, A. Javey, R. Tu, J. Cao, Q. Wang, and H. Dai, *Appl. Phys. Lett.* **87**, 173101 (2005).
- <sup>91</sup>Y. He, J. Zhang, Y. Wang, and Z. Yu, *Appl. Phys. Lett.* **96**, 063108 (2010).
- <sup>92</sup>Y. Noshio, Y. Ohno, S. Kishimoto, and T. Mizutani, *Nanotechnology* **17**, 3412 (2006).
- <sup>93</sup>L. Ding, S. Wang, Z. Zhang, Q. Zeng, Z. Wang, T. Pei, L. Yang, X. Liang, J. Shen, Q. Chen, R. Cui, Y. Li, and L.-M. Peng, *Nano Lett.* **9**, 4209 (2009).
- <sup>94</sup>J. Knoch and J. Appenzeller, *Phys. Status Solidi* **205**, 679 (2008).
- <sup>95</sup>Y. Noshio, Y. Ohno, S. Kishimoto, and T. Mizutani, *Appl. Phys. Lett.* **86**, 073105 (2005).
- <sup>96</sup>S. Nakamura, M. Ohishi, M. Shiraishi, T. Takenobu, and Y. Iwasa, *Appl. Phys. Lett.* **89**, 013112 (2006).
- <sup>97</sup>A. D. Franklin and Z. Chen, *Nat. Nanotechnol.* **5**, 858 (2010).
- <sup>98</sup>H. Michaelson, *J. Appl. Phys.* **48**, 4729 (1977).
- <sup>99</sup>D. Casterman, M. M. D. Souza, A. Tahraoui, C. Durkan, and W. I. Milne, *Phys. Rev. B* **79**, 125407 (2009).
- <sup>100</sup>S. Moon, S.-G. Lee, W. Song, J. S. Lee, N. Kim, J. Kim, and N. Park, *Appl. Phys. Lett.* **90**, 092113 (2007).
- <sup>101</sup>D. J. Perello, W. J. Yu, D. J. Bae, S. J. Chae, M. J. Kim, Y. H. Lee, and M. Yun, *J. Appl. Phys.* **105**, 124309 (2009).
- <sup>102</sup>R. W. Strayer, W. Mackie, and L. W. Swanson, *Surf. Sci.* **34**, 225 (1973).
- <sup>103</sup>H. Ishii, K. Sugiyama, E. Ito, and K. Seki, *Adv. Mater.* **11**, 605 (1999).
- <sup>104</sup>N. Park and S. Hong, *Phys. Rev. B* **72**, 045408 (2005).
- <sup>105</sup>X. Cui, M. Freitag, R. Martel, L. Brus, and P. Avouris, *Nano Lett.* **3**, 783 (2003).
- <sup>106</sup>S. Suzuki, C. Bower, Y. Watanabe, and O. Zhou, *Appl. Phys. Lett.* **76**, 4007 (2000).
- <sup>107</sup>J. P. Sun, Z. X. Zhang, S. M. Hou, G. M. Zhang, Z. N. Gu, X. Y. Zhao, W. M. Liu, and Z. Q. Xue, *Appl. Phys. A* **75**, 479 (2002).
- <sup>108</sup>M. Shiraishi and M. Ata, *Carbon* **39**, 1913 (2001).
- <sup>109</sup>M. Freitag, M. Radosavljevic, Y. Zhou, A. T. Johnson, and W. F. Smith, *Appl. Phys. Lett.* **79**, 3326 (2001).